

**New methods for preparing, imaging and typifying desmids (Chlorophyta, Zygnematophyceae), including extended depth of focus and 3-D reconstruction**

DAVID G. MANN<sup>1\*</sup>, MICHA M. BAYER<sup>1</sup>, STEPHEN J.M. DROOP<sup>1</sup>, Y.A. (JULIA) HICKS<sup>2</sup>,  
A. DAVID MARSHALL<sup>3</sup>, RALPH R. MARTIN<sup>3</sup> AND PAUL L. ROSIN<sup>3</sup>

<sup>1</sup>*Royal Botanic Garden Edinburgh, Edinburgh EH3 5LR, Scotland, UK*

<sup>2</sup>*School of Engineering, Cardiff University, Queen's Buildings, Newport Road, P.O. Box 925, Cardiff, CF24 0YF, Wales, UK*

<sup>3</sup>*School of Computer Science, Cardiff University, Queen's Buildings, Newport Road, P.O. Box 916, Cardiff CF24 3XF, Wales, UK*

\* Corresponding author ([d.mann@rbge.org.uk](mailto:d.mann@rbge.org.uk)).

RRH: Mann *et al.*: Desmid preparation and imaging

Keywords: Chlorophyta, desmids, extended depth of focus, imaging, microscopy, taxonomy, typification, World-Wide Web, Zygnematophyceae

D.G. MANN, M.M. BAYER, S.J.M. DROOP, Y.A. HICKS, A.D. MARSHALL, R.R. MARTIN AND P.L. ROSIN. 2006. New methods for preparing, imaging and typifying desmids (Chlorophyta, Zygnematophyceae), including extended depth of focus and 3-D reconstruction. *Phycologia* 00: 000–000

Species- and genus-level taxonomy of desmids depends largely on shape and detail of the cell wall and chloroplast morphology. The depth of most desmid semicells, relative to the focal depth of conventional light microscopes, means that morphological characteristics are usually illustrated by drawings, made from material that is mounted in water to allow re-orientation of specimens to different aspects of shape and pattern. Though a productive approach for two centuries, this has the disadvantages that features not initially detected or thought irrelevant are not recorded, drawing quality is variable, and individual specimens are rarely retained for further study. We describe methods for making permanent preparations of desmid cell walls and using these to produce extended depth of focus summary images and 3-D reconstructions. Together with World-Wide Web dissemination of image stacks, these advances make it practical to make a desirable change from typification via drawings to typification via single or multiple preserved specimens. They will also facilitate standardization of taxon concepts and identification.

## INTRODUCTION

Most desmids (Chlorophyta) are unicellular and have a cell wall consisting of two halves termed semicells. According to Růžička (1977) and Brook (1981), desmids comprise five families, which are classified in the class Zygnematophyceae (van den Hoek *et al.* 1995; formerly Conjugatophyceae) or order Zygnematales (Graham & Wilcox 2000). The 'saccoderm' desmids (family Mesotaeniaceae) are usually simple cylindrical cells without external wall ornamentation and they lack the median constrictions or sutures that are typical of the 'placoderm' desmids (families Gonatozygaceae, Peniaceae, Closteriaceae, Desmidiaceae: Brook 1981). Kouwets & Coesel (1984) recommended that the Gonatozygaceae are combined with the Peniaceae but this is not consistent with *rbcL* (McCourt *et al.* 2000) or 18S rDNA (Gontcharov *et al.* 2002) sequence data. The placoderm desmids have a more complex wall structure than the saccoderms and possess elaborate systems of pores. Cell shape, size and wall patterning are highly constant within species or species groups and have been the primary basis for generic and species-level classification, together with aspects of chloroplast morphology. Molecular systematic studies, e.g. by McCourt *et al.* (2000), Gontcharov *et al.* (2002) and Gontcharov & Melkonian (2005) show that aspects of the current taxonomy are unsatisfactory at the family and genus level. However, although molecular approaches are necessary to establish a natural classification, morphology remains central to species-level desmid systematics and identification, and accurate illustrations are therefore important.

Desmid cells are cylindrical to multiradiate (Brook 1981) and the main body of the cell may bear many hollow processes. The complexity of the shape in many species, and the fact that each semicell is many times deeper than the depth of focus of a high numerical aperture lens in even the smallest and flattest species, means that it has always been difficult to make adequate illustrations of desmids in two dimensions. Drawings have several advantages over photographs in this context: they can (1) represent the whole specimen in focus, by combining information from many different focal planes; (2) represent the features that the artist wants the reader to see, without the picture being cluttered with 'irrelevant' detail, such as the nucleus; and (3) illustrate the specimen in standard elevations (specimens rarely settle perfectly level), facilitating comparison. A good earlier example of the use of drawings is West & West's (1904–1923) account of British Desmidiaceae (now available on the web as a searchable database at

[http://rbg-web2.rbge.org.uk/DIADIST/ww\\_intro.htm](http://rbg-web2.rbge.org.uk/DIADIST/ww_intro.htm)) and all the major recent floras (e.g. Bicudo & Azevedo 1977; Bicudo & de Castro 1994; Bicudo & Samanez 1984; Bicudo & Sormus 1982; Bourrelly & Couté 1991; Coesel 1982, 1983, 1985, 1991, 1994, 1997; Compère 2001; Croasdale & Flint 1986, 1988; Croasdale *et al.* 1983, 1994; Förster 1982; John *et al.* 2002; Lenzenweger 1996, 1997, 1999, 2003; Prescott *et al.* 1972, 1975, 1977, 1981, 1982; Růžička 1977, 1981) follow suit. However, to produce good drawings requires rare skills in observation, interpretation and manual dexterity, and considerable time.

Reorientation of a specimen for photography or drawing in standard orientations can be achieved by mounting cells in a liquid medium and flicking the cell repeatedly (e.g. by tapping the coverslip with a dissecting needle) until it adopts the next required position. However, liquid mounts are ephemeral and so the specimens illustrated are subsequently lost; even where care is taken to seal a preparation, eventually the material dries out (e.g. Dingley 2003). Hence the type of each desmid species, variety or form (and desmids are particularly rich in varieties and forms) is usually only a drawing and original specimens cannot be re-examined during taxonomic revision, nor are they available to facilitate identification by ecologists. Recent papers describing new desmid taxa by Couté & Dehbi-Zebboudj (1988), Bourrelly & Couté (1991), Kouwets (1991), Gerrath & John (1991), Kim (1996), Coesel (1996) and Williamson (1997) all use drawings to typify desmid taxa, although Couté & Dehbi-Zebboudj (1988, building on earlier work by Couté & Tell 1981), also include scanning electron micrographs and Hegewald & Fehér (2003) use such images as types. The same problem affects most microalgae and flagellates, which are generally typified by drawings or photographs.

Typification can be problematic even where long-term preservation is easy, as in the diatoms, where whole slide preparations containing 10s or 100s of taxa have traditionally been used as types rather than individual specimens (Mann 1998). Here, because several related species often occur together, it can be difficult to be sure exactly what an author had been looking at when he or she described a particular taxon (cf. Mann 2002). The application of many typified names is therefore unclear, which is exactly what typification is meant to avoid. We have therefore recommended that individual specimens are designated as types, not slides (e.g. Droop 1996; Mann 2002). For this to be possible, however, specimens must be immobilized and mounted permanently, so that they can be relocated, e.g. using a

finder slide. The need for this in desmids can be illustrated via the *Staurastrum* in Fig. 1. This specimen agrees reasonably well with *S. teliferum* Ralfs, but it is also like *S. gladiusum* Turner and *S. subteliferum* Roy & Bissett (Hegewald & Feher 2003 indicate that this group of species is taxonomically difficult). Careful focusing reveals that the semicell apex has a central pore, surrounded by a ring of nine regularly arranged pores (and possibly a second, more irregular ring). All the pores are extremely faint and they are not evident in the drawings of e.g. West & West (1904–1923). However, it is impossible to say whether most previous authors did not record pores (1) because they were too difficult to detect, or (2) because none were present, in which case our *Staurastrum* might represent an undescribed taxon, or (3) because the same pattern of pores occurs in all *Staurastrum* species of similar shape (cf. Gerrath 1993, p. 110), so that pores have no diagnostic value and drawing them is superfluous. Williamson [1996, fig. 14(4)] is an exception among desmidiologists because he does illustrate pores on the semicell apices of several *Staurastrum* species, including *S. teliferum*. Among the species he illustrated there are several pore patterns – arguing against possibility (3) above – and, whereas *S. teliferum* is shown as possessing a central pore surrounded by a ring of pores, the number of pores in Williamson’s material differs from that in our specimen (11, not 9) and outside this ring there are many pores between it and the spine bases, rather than a single irregular ring. The identification of our specimen is therefore uncertain and cannot easily be checked against authenticated or type material.

It would be beneficial, therefore, to (1) prepare permanent preparations of desmid cell walls, so that particular specimens remain available for further study, (2) find ways to visualize cell walls that combine the advantages of drawings (e.g. that information can be combined from different focal planes) with those of photographs (subtlety, positional accuracy, completeness, less variation due to artistic style), and (3) have some capacity to rotate images in all directions, to determine three-dimensional (3-D) structure and allow comparison with specimens that do not have the same orientation. These three would facilitate a change to specimen-based, as opposed to image-based, typification of desmids. Our aim here, therefore, is to document a new method for harvesting desmids and preserving them immobile in a durable mounting medium, so that specimens can be relocated for future re-examination, and to demonstrate how such immobilized specimens can be used to maximum effect as types. We also indicate how summary images might in future be used for automated identification.

## MATERIAL AND METHODS

### Sample collection

EPIPELIC SPECIES. The top 1–2 cm of exposed or submerged sediments were removed, together with overlying water, using a glass tube (Round 1953) or a small shovel. Enough was collected to fill a two-litre screw-cap plastic bottle. Samples were kept cool in an ice-box to minimize decay during transport. In the laboratory, sediment was resuspended by gentle shaking and poured into a flat tray (c. 0.25 m<sup>2</sup>) to produce a sediment thickness of 1–2 cm after settling. After the suspended sediment and algae had settled for at least 3 h (usually in the dark to ensure that motile algae remained mostly within the sediment), water above the sediment was removed with a water suction pump, with minimal disturbance of the sediment. Two layers of lens tissue were then placed on the sediment, to cover its entire surface, and strips of clear polythene (1–2 cm wide, from polythene sample bags) were laid on top of the lens tissue as traps for algae, leaving 1–2 cm gaps between the strips for aeration of the sediment. The trays of sediment were placed in daylight (but out of direct sunlight), or under continuous light in an incubator (at 5–50  $\mu\text{mol photons m}^{-2} \text{s}^{-1}$ ), and covered with a glass sheet to prevent desiccation. Motile algae migrated out of the sediment, through the lens tissue (acting as a filter), onto the polythene. The next day, the polythene strips were removed and the cells adhering to them were harvested with a sterile cell scraper, producing a concentrated slurry of desmids, diatoms and other algae. Where yields were low, the polythene strips were replaced on the sediment on areas previously left clear, left overnight, and used again for harvest the following morning.

PLANKTON AND METAPHYTON: Planktonic desmids were sampled using a 25  $\mu\text{m}$ -mesh plankton net repeatedly thrown out from the shore. A net of similar mesh size, mounted on a broom handle, was used for hand sweeps of the metaphyton loosely associated with the marginal macrophytes of ponds and lakes. Larger organisms (e.g. crustaceans) and debris were removed by sieving (c. 500  $\mu\text{m}$  mesh size) and material was fixed soon after collection to reduce grazing by residual zooplankton. Desmids also occur associated with moss carpets (e.g. *Sphagnum*, *Calliergon*, spp.) in permanently damp areas; to sample these, handfuls of moss were removed and allowed to drain for a few seconds to remove most of the water. The moss was then squeezed into a sample bottle, via a funnel, and strained as above to remove grazers and plant fragments.

## Preparation protocols

Formalin was added to give a final concentration of 4% formaldehyde and the sample left overnight. Material can be preserved long-term in the fixative.

Our slide preparation protocol requires transfer of material through several solutions and we used sedimentation to separate the desmids from the medium. This was more time-consuming than centrifugation but produced less damage. We sedimented material for c. 6 h, which was enough for small desmids to sink to the bottom. Unfortunately, it also allowed small particles of debris to settle and hence to be included in the slides. Even using sedimentation, some cells still became damaged or distorted, because the cleared cells were extremely fragile and deformed more easily than fixed whole cells, which have the internal support of the fixed protoplast.

A subsample of fixed material was transferred to a straight-sided, flat-bottomed, 10 ml glass vial with a tight fitting plastic lid, topped up with distilled water, mixed by inverting several times, and allowed to settle for 6 h. The supernatant was carefully removed by pipette, leaving only a small meniscus of liquid above the sedimented sample. The tube was refilled with distilled water, again allowed to settle for 6 h, and the supernatant removed, leaving a visible meniscus. The tube was then filled with 10 ml of 5% sodium hypochlorite ( $\text{NaOCl}$  = household bleach) solution and sonicated in a water bath for 3 min. The tube was left to settle overnight and the bleach removed by pipette, and then the bleached material was washed with distilled water as above. After settling for 6 h, as much as possible of the supernatant was removed and replaced by 10 ml 96% ethanol. The sample was mixed gently and left to settle for 6 h. The supernatant was then removed, leaving approx. 1 ml of sample, and an equal amount of Euparal essence added, mixed by inversion and left for 10 min. The sample was then spun down in a bench top centrifuge at 6500 rpm for 2 min, as much as possible of the supernatant removed, and pure Euparal essence added, adjusting the amount to suit the sample concentration and intended density of algae on the slide. Finally, an equal volume of Euparal mountant was added to the sample–Euparal essence mixture and mixed by gentle uptake and expulsion from a pipette until the two phases were no longer recognizable as separate.

Slide preparations were made by pipetting 15–20  $\mu\text{l}$  of sample mix onto a slide and covering with an 18  $\times$  18 mm coverslip, taking care to avoid trapping

bubbles. Slides were dried flat for a minimum of 5 days at room temperature or for 3–5 days on an electric drying tray at 50°C.

### **Microscopical methods and production of image stacks**

In order to capture all detail visible in a desmid with the light microscope, digital or other images need to be taken using high numerical aperture lenses (to give maximum  $x$ - $y$  resolution) at sufficient magnification to match the camera resolution (Bayer *et al.* 2001), and optical sections need to be at a vertical ( $z$ ) spacing of *c.* 0.2  $\mu\text{m}$  (see below, ‘Depth of focus’). We used a Reichert Polyvar 2 photomicroscope (Reichert–Jung, Vienna, Austria) fitted with a Polaroid DMC2 digital camera capable of  $1600 \times 1200$  pixel resolution. Desmids were photographed using oil immersion lenses of  $\times 40$  [Numerical Aperture (NA) = 1.0] or  $\times 100$  (NA = 1.32 or 1.30), with an appropriate setting of the intermediate magnification changer (0.8, 1, 1.25 or 2) and bright field, phase contrast or differential interference contrast optics. Image stacks were obtained manually. The fine focus control of the Polyvar is marked in 1  $\mu\text{m}$  steps, each about 1 mm apart and representing a rotation of the control of around  $3^\circ$ . We therefore constructed and attached a vernier scale, such that ten intervals occupied the same arc as nine divisions (9  $\mu\text{m}$ ) of the fine control. Aligning each of the lines on the vernier scale in turn with a line on the fine focus control allowed capture of optical sections at 0.1  $\mu\text{m}$  intervals of vertical movement of the stage (although, in practice, we mostly took sections at 0.2  $\mu\text{m}$  intervals). Thus, even a small- or medium-sized desmid will produce a large image stack, comprising several tens of images.

Because of refraction at interfaces between materials of different refractive index along the optical path, physical vertical intervals do not correspond to optical intervals. This can be avoided only if the mountant and the medium between cover-slip and objective (here, immersion oil) have the same refractive index (RI). Pluta

(1993, p. 36) gives the formula  $t = t' \left[ \frac{n' - \sqrt{n'^2 - A^2}}{n - \sqrt{n^2 - A^2}} \right]$ , where  $A$  is the numerical

aperture of the objective,  $n'$  is the RI of the immersion fluid between cover-slip and objective,  $n$  is the RI of the object (essentially the mountant in our case),  $t$  is the real geometrical depth of the object, and  $t'$  is the observed depth (measured by movement of the fine focus control). Our protocol employed Euparal with RI = 1.48. If so, with immersion oil of RI = 1.515 and a 1.32 NA objective lens, the actual depth interval

between optical slices will be 0.190  $\mu\text{m}$ , not the measured 0.2  $\mu\text{m}$  (applying the formula given above gives an actual depth of 95.2% of the measured depth; if the condenser is not oiled to the slide, the actual depth is 96.4% of the measured depth, for the optical system specified above). In a water mount (RI  $\sim$ 1.33), the difference between real and apparent depth is much greater, a 0.2  $\mu\text{m}$  apparent interval being equivalent to 0.132  $\mu\text{m}$  real depth (66.1% of the measured depth).

### **Depth of focus and diffraction artifacts**

High numerical aperture (NA) lenses have a low depth of focus. For example, using the formula for diffraction-limited systems given by Young *et al.* (1993), the 1.32 NA apochromat we used has a depth of focus of 0.178  $\mu\text{m}$  in green light of  $\lambda = 550$  nm. Hence, a single photographic image (or even several images) cannot convey all salient information about desmid morphology; consequently, it has not previously been practical to illustrate desmids photographically for taxonomic purposes. We therefore developed software to produce a single in-focus image from a stack of thin optical sections, using normal (as opposed to confocal scanning) microscopy. This appears to offer significant improvement over currently available commercial software and freeware. We also developed software to allow us to rotate the in-focus image to produce standard elevations, to minimize the disadvantage that permanently mounted semicells cannot be physically reorientated.

The principal problem hindering the production of a single, high quality, in-focus image from a stack of optical sections of a microalga is diffraction. With macroscopic objects and at low magnifications of the microscope, the effects of diffraction in image formation can be largely ignored. Consequently, image combination methods that look for and retain in-focus parts of an image through some form of maximum contrast algorithm can produce a focused summary image from a stack. This is not so easy in diffraction-limited optical systems, as during use of high numerical aperture lenses, because in transparent objects, where the image consists only of edges made visible by differences in refractive index, diffraction leads to the formation of two or more in-focus images at different levels. These differ in intensity relative to the background illumination, appearing either light or dark. As a consequence, any algorithm that selects for in-focus parts of an image will find multiple versions that, if summed, will largely cancel each other through destructive interference.

We illustrate this in Fig. 2, which shows a single optical section near the surface of a desmid prepared using our new protocol and photographed using bright field optics. For the objective used (NA 1.32), Young *et al.*'s (1993) formula gives a depth of focus of 0.18 or 0.26  $\mu\text{m}$ , depending on whether the condenser (NA 1.3) is oiled or not, respectively (Bradbury 1984), and so little of the specimen is in focus. The specimen, being made essentially of cellulose, has a higher RI (1.56: Frey-Wyssling 1976, p. 169) than euparal (1.48–1.52). Parts of the specimen fractionally below the focal plane of the microscope appear in-focus as light regions surrounded by a dark halo (e.g. the two right hand arms of the desmid in Fig. 2), whereas features fractionally above the focal plane appear in-focus as dark regions with a light halo (e.g. the two left hand arms in Fig. 2). At the precise focal plane of the microscope, the feature disappears completely as the phases reverse. Figure 4 shows this directly for a photographically small spherical object (*c.* 1  $\mu\text{m}$  diameter, with a higher refractive index than the mountant), as a vertical 'section', reconstructed from a series of optical sections (see the section '3-D reconstruction...' below for explanation). The object is imaged sharply in two planes (Fig. 4, arrows), separated by a narrow zone in which there is no contrast between object and background. Around each principal focus (white or black), there is a cone of opposite phase (dark or light, respectively), which is the 'halo' seen in the  $x$ - $y$  plane. Figure 6 shows the changeover from white to black focus in a ring of papillae that lay slightly oblique to the image plane.

The order in which the dark and light foci appear in bright field optics is dependent on the relative refractive indices of the object ( $RI_{\text{obj}}$ ) and mountant ( $RI_{\text{m}}$ ). Where  $RI_{\text{obj}} > RI_{\text{m}}$ , the light focus appears above the dark (i.e. the object will appear pale when the focal plane of the objective is above it), as in Fig. 4 and the desmids illustrated in this paper. However, where  $RI_{\text{obj}} < RI_{\text{m}}$ , as with diatoms (RI 1.4–1.43: Lewin 1962) mounted in either euparal, Canada balsam (RI 1.52–1.54: Budavari 1989) or Naphrax (RI 1.7: Fleming 1954), the dark focus lies above the light.

Figure 3 is of the same desmid as in Fig. 2 (and at approximately the same focus), but this time photographed using phase contrast optics. In this case, three in-focus images of each element of structure are formed and Fig. 5 illustrates their spatial relationship for a small spherical object (*cf.* Fig. 4). Precisely at the focal plane of the objective lens, a feature appears in sharp dark focus (the primary focus) relative to the background, e.g. in the upper left-hand arm in of the desmid in Fig. 3.

Focusing above or below the feature causes it to disappear for a considerable vertical interval (Fig. 5) before it reappears in focus, now light against the background; however, the two secondary foci are not as intense or as sharp as the primary focus. The right-hand arms in Fig. 3 are almost in secondary white focus below the focal plane, whereas the isthmus (the circle in the middle of Fig. 3) is more or less in secondary focus above the primary focal plane, both being light relative to the background. Outside the two light foci, in either direction, the feature gradually becomes blurred. As with bright field optics, the production of light and dark foci depends on the relative RIs of object and mountant. For diatoms in euparal, Canada balsam or Naphrax, where  $RI_{obj} < RI_m$ , the primary focus shows the diatom light against a dark background, whereas the two secondary foci show it dark against a light background.

The series of optical sections from which Figs 2 and 3 were taken can be viewed and interactively focused on-line at [http://rbg-web2.rbge.org.uk/DIADIST/focus/des\\_focus.htm](http://rbg-web2.rbge.org.uk/DIADIST/focus/des_focus.htm), which also includes a stack of optical sections taken using differential interference contrast optics.

The problem is therefore to find a way to discriminate between the two or three sets of alternative in-focus images that diffraction creates, so that a single consistent set can be selected and used to construct a composite, wholly in-focus image, either white against black or black against white. Failure to do so may lead either to loss of features or creation of deceptive artifacts (the diatom fragment at the top in Fig. 31 shows an apparent doubling of the striae near the margin, which was produced during image processing; contrast Fig. 32).

### **Computation of an extended depth of focus (EDOF) image**

There have been several recent attempts to develop algorithms to produce wholly in-focus (EDOF) images of a 3D object from sets of digital optical slices (Burt & Kolczynski 1993; Li *et al.* 1995; Valdescas *et al.* 2001; Hill *et al.* 2002).

Furthermore, for each pixel in the EDOF image, it is possible to estimate to which slice it is most likely to belong, potentially allowing reconstruction and rotation of the 3D structure. As noted in the previous section, however, microscopic objects with structural details of  $\sim 0.5 \mu\text{m}$  present special difficulties because of diffraction. Certain types of artifact produced by diffraction, such as blurring, can be modelled using a point spread function and successfully removed using deconvolution techniques (Gonzalez & Wintz 1987). However, modelling and removing other

artifacts, such as the multiple-focus problem described above and the related ring artifacts seen around objects, requires a more sophisticated approach, involving a very difficult inverse problem – essentially we would need to determine the structure of the object before the artifacts could be isolated and removed. To the best of our knowledge, this has not been done. We have instead taken a pragmatic approach, developing algorithms that allow the multiple focus problem to be circumvented by pre-processing each picture in a stack before detection of in-focus areas in each image.

**PRE-PROCESSING:** Because there are alternative foci differing in phase, a particular feature may be lost by cancellation during assembly of in-focus parts of a stack. To avoid this, we preprocessed the images to remove the ‘white focus’ part of each image, in which features are pale against a darker background. Two methods gave good results.

The first method (PP1) calculated the average grey level for each depth column of pixels in the stack. Then, for each pixel in each image whose grey level was above the corresponding average value for the column to which it belonged, we subtracted twice the difference between its value and the corresponding average. This operation ‘mirrors’ the light grey values about the average. Thus we turned areas of light focus into areas of dark focus while retaining most of the information to be used in the next stage, where the image slices are combined into a single in-focus image. The effect is shown by comparing Figs 6 and 7. In the original image (Fig. 6), a ring of papillae near the isthmus of *Staurastum cf. polymorphum* appears in black focus at the left, but in white focus at the right, because the ring lay slightly oblique to the focal plane of the microscope. PP1 changes the white-focus papillae into dark spots (Fig. 7, arrows). A disadvantage is that narrow dark haloes are created around the papillae originally in dark focus (Fig. 7, arrowhead).

The second method (PP2) was an adaptive thresholding method, whereby each pixel whose grey level was above (i.e. paler than) a threshold was given the same grey value as the threshold. The choice of threshold depended on the spread of grey level values among all pixels in all image slices. We tried several threshold values: (1) the average grey level (PP2.1); (2) one standard deviation below the average grey level (PP2.2); and (3) one standard deviation above the average grey level (PP2.3). Figure 8 shows the effect of the PP2.1 method. Those papillae on the left that originally appeared black (Fig. 6) remain almost unaltered in appearance

after pre-processing, whereas those on the right disappear. Elsewhere in the stack, the reverse was true, the papillae on the right being retained but those on the left being deleted.

EXTENDED DEPTH OF FOCUS ALGORITHMS: Algorithms to produce EDOF images (Burt & Kolczynski 1993; Li *et al.* 1995; Valdescas *et al.* 2001; Hill *et al.* 2002) can be classified into those that work on a point basis, those that work on an area basis, and those that work in the frequency space of the images obtained through the Fourier or wavelet transforms (a wavelet transform is similar to a Fourier transform but is localized to parts of an image; for more detail, see Burke Hubbard 1996). The latter methods fuse images to obtain a fully in-focus image, not by combining pixels from the different images, but by combining Fourier or wavelet coefficients obtained from the different images and then performing an inverse Fourier or wavelet transform on the combined coefficients to obtain the EDOF image. Valdescas *et al.* (2001) and Hill *et al.* (2002) compared different methods quantitatively and found that methods working in wavelet space generally gave the best results. Hill *et al.* employed a complex wavelet transform, which they showed gives the best results when combined with a local window voting scheme. Valdescas *et al.* showed that combining wavelet-based EDOF algorithms with voting schemes over a small window provide the best results. In this article, we use Hill *et al.*'s Matlab (Natick, Massachusetts, USA; <http://www.mathworks.com/>) implementation of the above methods, viz. a method based on complex wavelet transform with additional consistency check (Hill *et al.* 2002). Their original method fused two images at a time. We modified it to allow us to combine more than two images, as well as to cope with the diffraction effects. Code for the EDOF algorithms is available at <http://www.cs.cf.ac.uk/diadist/Fusion.zip>.

WHOLE AND PARTIAL STACKS: For each desmid semicell, the EDOF programs were initially run on the whole image stack. Hence, features from both surfaces (upper and lower) were superimposed in the EDOF images. We also ran the programs on some partial stacks, representing only part of the vertical depth of the semicell or cell and containing only one of the two surfaces. A slight overlap between partial stacks was often desirable, to ensure that the complete outline of a semicell or cell was recovered.

### **3-D reconstruction and rotation**

We used two approaches to reconstruct 3-dimensional objects from a stack of equidistant parallel optical sections and visualize them from a new viewpoint.

MODEL 1: Each 2-dimensional pixel in an optical section was treated as a 3-D 'voxel' of the whole stack. To do this, the actual vertical interval of the optical sections must be known. For our optical system the actual vertical interval between sections is 95.2% of the measured interval (see 'Microscopical methods'). Hence, for 0.1  $\mu\text{m}$  measured vertical interval, the actual interval is 0.095  $\mu\text{m}$  (calculated according to Pluta 1993). Each picture in a through-focus image stack was then resampled digitally (using bicubic interpolation in Adobe Photoshop: Adobe Systems, San Jose, California, USA: <http://www.adobe.com/products/photoshop/>) so that the  $x$  and  $y$  dimensions of each pixel approximately matched the 0.095  $\mu\text{m}$  vertical interval. The resulting voxels were therefore approximately cubes. The voxels in a through-focus series ( $z$  pictures, each of  $x \times y$  pixels) were then rearranged into two orthogonal series of reconstructed pictures, one of  $x$  pictures (each of  $z \times y$  pixels), the other of  $y$  pictures (each of  $z \times x$  pixels). The new stacks along the  $x$  or  $y$  axes could then be run through the EDOF algorithms, like the original stack along the  $z$  axis. Such new pictures show the specimen in side view. Alternatively, single  $x$ - $z$  or  $y$ - $z$  slices can be viewed and this is how the illustrations of the effects of diffraction (Figs 4, 5) were produced.

MODEL 2: All pixels in a stack of photographs were binary coded on the basis of sharpness: the in-focus pixels in each optical section were treated as 'present' and all other pixels treated as 'absent'. The 'present' pixels (principally those on the surface of the desmid) were then given  $x$ ,  $y$ ,  $z$  coordinates according to their position, which were then fed (as ASCII values) into a graph-drawing program (e.g. SigmaPlot, version 8.0.2: Systat Software, Point Richmond, California, USA; <http://www.systat.com/products/SigmaPlot/>), and plotted as a 3-D graph. This could be rotated and hence viewed from different angles. More sophisticated approaches could be taken to 3-D modelling, using the  $x$ ,  $y$ ,  $z$  coordinates, e.g. by connecting them in a continuous smooth surface, but our simpler approach is sufficient to demonstrate any potential benefit.

## **RESULTS**

### **Desmid permanent mounts**

Figures 9–23 show examples of desmids prepared using the new protocol and photographed using a  $\times 40$  oil immersion lens. Fine detail of pores and wall ornamentation are evident (e.g. Figs 1, 12, 13, 23). Both whole cell walls (Figs 11–19) and separated semicells (Figs 9, 10, 20–23) remained after cleaning with bleach. In both cases cell contents were often absent, but sometimes small residual masses of material remained (e.g. at the centre in Figs 29–32). Not all specimens were as well preserved as those shown. Some were folded or bent, especially flimsy members of the Closteriaceae, and walls sometimes cracked during preparation (Fig. 12). Contrast between wall and mountant was low. Differential interference contrast or phase contrast optics are therefore helpful, and contrast could be increased further by using high refractive index mountants generally used for diatoms, such as Naphrax. However, with modern digital contrast-enhancement methods, low contrast is not a major problem, providing it is sufficient to allow accurate focusing.

#### **Extended depth of focus images**

The results of applying EDOF algorithms to image stacks of desmids prepared using the new protocol were tested using four image stacks, representing *Staurastrum* cf. *polymorphum* and *S. cf. teliferum* viewed with bright field and phase contrast optics. The nominal vertical separation of images (see above, ‘Microscopical methods and production of image stacks’) was 0.5  $\mu\text{m}$  for *S. cf. polymorphum* (stacks of 51 and 40 images for bright-field and phase-contrast, respectively) and 0.2  $\mu\text{m}$  for *S. cf. teliferum* (stacks of 190 and 120 images for bright-field and phase-contrast). Stacks of images were somewhat greater than the actual depth of the specimen required, in order to allow proper assessment of the effects of pre-processing on the multiple focus problem (because of vertical flare of the image: Figs 4, 5).

The untreated outputs had very low contrast. For Figs 24–32, we therefore altered global brightness and contrast using the Brightness/Contrast or Levels tools in Photoshop, without dodging or burning particular areas. Enhancement tended to produce rather grainy images, especially for bright-field images (Figs 24–26, 28, 30), because the amplitude of any noise in the pictures (introduced, for example, during image capture with the Polaroid DMC2 camera) was increased by stretching the dynamic range of the subject matter.

Figure 24 shows an EDOF image of *S. cf. polymorphum* prepared without pre-processing from the same stack of bright-field images used for Figs 25 and 26. Comparison with other reconstructions of the same semicell of *S. cf. polymorphum*

(Figs 25–28 and especially Figs 34, 35) show that the white focus–black focus conflict has led to significant loss of detail, especially near the outline of the semicell and in the arms, and many papillae are blurred. The need for pre-processing is evident.

BRIGHT FIELD STACK OF *STAURASTRUM* CF. *POLYMORPHUM* (FIGS 25, 26): The specimen of *S. cf. polymorphum* – a semicell seen from its apex – had four truncate arms covered with small papillae, both on the distal side and on the side nearest the isthmus. The isthmus was surrounded by a neat ring of papillae (Fig. 6). The EDOF images combine information from both surfaces of the semicell, so that the isthmus ring is partially disguised among the papillae on the distal face of the semicell.

Although we tried all three variants of PP2 on both series of sections, in Fig. 26 we illustrate only PP2.1, in which the adaptive threshold was set to the average grey level of all the pictures in the series. PP1 and PP2.1 produced similar images. The outline of the semicell is almost complete, becoming faint only at the tips of the arms. The position of the isthmus is clear, though its outline is incomplete on the right. One difference between PP1 and PP2.1 is that in the PP1 EDOF image (Fig. 25), there are narrow white haloes around dark objects such as individual papillae (cf. Fig. 7) and (though to a lesser extent) around the perimeter of the desmid. This is more truthful to the original images because, as Fig. 4 shows, diffraction produces symmetrical fringes (haloes) around any small object, of which the first is by far the strongest; so, a papilla in dark focus is surrounded by a prominent white halo. PP2.1 suppresses the white halo (Fig. 26; cf. Fig. 8), but at the expense of some clarity. The PP1 image is therefore sharper and the papillae are rendered more or less consistently, whatever their position relative to the margin in the original image; a few papillae are lost in the PP2.1 image. On the other hand, although white haloes are a real feature of the original images in the stacks, they are optical artifacts (for example, they are not areas where the cell wall is thinner or inflected) and their suppression by PP2.1 can be regarded as a virtue.

The results from PP2.2 and PP2.3 (not illustrated) were slightly worse. Using PP2.2 (with the threshold set below the average grey level), the result was sharp but incomplete, the ends of the arms being barely visible. With PP2.3 (with the threshold set above the average grey level), the semicell outline was more complete but less sharp. This is understandable, because the average grey level of the whole stack will tend to be the grey level at the *z* plane equidistant from the light and dark in-focus

images of any element of structure (Figs 4, 5). So, with the threshold set below the average (PP2.2), only the most intense black phase information will be included in the processing; thus (1) the fainter details are lost, (2) those details that are retained are shown very sharply without the diluting influence of the white phase, and (3) the backgrounds tend to be slightly less noisy. With the threshold grey level set above the average (PP2.3), some of the white-phase information in each picture is processed, so that (1) faint dark details are detected more easily, but (2) sharpness is reduced slightly, because of the diluting influence of information from the white phase, and (3) the backgrounds tend to be slightly more noisy.

PHASE CONTRAST STACK OF *STAUSTRUM* CF. *POLYMORPHUM* (FIGS 27, 28):

The phase contrast stacks, having greater initial contrast, yielded less grainy and hence more visually attractive EDOF images, but these did not necessarily contain more morphological information. All features are in focus and well visualized in the PP1 image (Fig. 27), though they are less crisp than in the equivalent bright field image (Fig. 25). The white halo gives clear definition to the cell outline and an almost three-dimensional appearance to the papillae at the ends of the semicell arms. The isthmus is more clearly visible than in any of the other tests. One undesirable feature of this image is that papillae are rendered somewhat inconsistently across the semicell, those near the margin of the semicell being less distinct than those lying nearer the centre and those seen in profile on the margin itself. Outside the margin, running more or less parallel to it, are a series of irregular arc-like fringes. In the PP2.1 EDOF image (Fig. 28), features are as well in-focus as in the PP1 phase contrast image and are more consistently rendered. However, the isthmus is less distinct. The cell outline is particularly well clear and of almost constant apparent thickness; this could be an advantage in morphometric analysis.

The PP2.2 image (not illustrated) appeared slightly better than the PP2.1 image because the background was almost noiseless; however, details of the desmid itself were no better than in PP2.1. PP2.3 gave a noticeably less sharp image than PP2.1 and 2.2.

BRIGHT FIELD STACK OF *STAUSTRUM* CF. *TELIFERUM* (FIGS 29, 30):

*Staurastrum* cf. *teliferum* semicells have wide, bluntly rounded or slightly polygonal arms. There are no papillae but instead the distal and proximal surfaces of the semicell bear long tapering spines, which are concentrated in a band around its maximum circumference.

After PP1 (Fig. 29) or PP2.1 (Fig. 30) processing, the spines are clearly in focus, except where they join the rest of the cell wall. The cell wall is in sharp focus in both cases, but it is more continuous in the PP2.1 image. PP1 gives a sharper outline to the isthmus than PP2, though the simple dark line around the aperture in PP2 is aesthetically superior and conveys an impression of the thickness of the wall. The results from PP2.2 and PP2.3 (not illustrated) were almost as good as the PP2.1 image, but with a slight loss of detail in PP2.2.

PHASE CONTRAST STACK OF *STAURASTRUM* CF. *TELIFERUM* (FIGS 31, 32): The PP1 and PP2.1 images for *S. cf. teliferum* differ more in overall character from each other than in the other three pairs we illustrate, but as elsewhere there is no clear 'winner'. The spines are sharply focused in both and the isthmus aperture is clearly visible. The outline of the cell body can be traced in both cases, but is discontinuous in the PP2.1 image (Fig. 32) and bordered by strong fringes in PP1 (Fig. 31); the bright-field EDOF images are preferable in this respect (Figs 29, 30). Some of the spines appear unconnected to the cell body in the PP2.1 image. The PP2.2 and PP2.3 results (not illustrated) were slightly worse than the PP2.1 image. PP2.2 produced a very sharp result showing the spines very clearly, but parts of the cell outline were missing. With PP2.3, the cell outline was better represented, but overall the image was less sharp.

COMPARISONS WITH SOME OTHER AVAILABLE ALGORITHMS: Most of our new EDOF images, whatever the algorithms used, surpassed the quality evident in an EDOF image (Fig. 33) kindly prepared for us by Dr Ian Harding (Southampton Oceanography Centre), using Auto-Montage software (Syncroscopy, Cambridge, UK). This image gives a good overall impression of cell shape, but surface spines are inconsistently rendered (some light, some dark) and parts of the image, particularly around the margin of the cell, are an obvious mosaic. The scale of the mosaic can be reduced using a smaller 'patch' size in Auto-Montage. The most recent version of Auto-Montage (version 5.01 demonstration version at <http://www.syncroscopy.com/>) seems to give some improvement over previous algorithms, but still rendered the outline poorly in phase contrast and produced almost nothing useful for our stacks of bright-field images (e.g. those used to produce Figs 25, 26, 29 and 30). InfiniteFocus Junior software package (<http://www.alicon.com/>) produced similarly inconsistent and mosaiced results, and many papillae were totally lost in reconstruction from the bright field stacks. We also failed to produce a usable image from our stacks using

the application developed by Forster *et al.* (2004; see also <http://bigwww.epfl.ch/demo/edf/index.html>).

### **Partial stacks and image improvement**

Providing that a specimen is lying with one of its major axes approximately parallel to the z axis of the stack, a stack can be subdivided so that the two sides of a desmid can be imaged separately. In the case of a desmid in apical view, this allows the production of two quite different images, showing the isthmus and cell apex, respectively. Figures 34 and 35 were derived from the same phase contrast image stack of *Staurastrum cf. polymorphum* as was used to produce Figs 27 and 28, but the original stack of 50 optical sections was divided into two substacks of 29 and 32 sections, with an overlap of 11 (~ 5  $\mu\text{m}$ ) to allow a complete outline to be formed in both. Both EDOF images have remarkable clarity.

Further examples of EDOF images, based on partial or complete stacks, are shown in Figs 36–42. Complete stacks have the advantage that the whole 3-dimensional shape is represented, allowing visualization of the complex morphology in some taxa (e.g. Figs 37, 38), and where a specimen is lying obliquely (Fig. 36), no subset of sections may be entirely satisfactory for EDOF reconstruction. However, where a desmid has a simple symmetrical shape, EDOF side views are often best obtained from partial stacks representing one side only (Figs 39–41). If this is not done and no information is given about the spatial origin of each element of the image, there is a risk of misinterpretation. For example, the subtle warts of Fig. 42, which is based on a whole stack, are not evident in EDOF images derived from stacks representing each side on its own, and the curious claw-like appearance of the cell apex is an artifact produced because in this specimen the apical notch that is characteristic of *Tetmemorus* lay oblique to the image plane. An almost identical orientation was drawn by Ralfs (1848, pl. 24, fig. 1c).

As already mentioned, our EDOF program outputs have very low contrast. Some of the pre-processing algorithms tend in addition to produce strong haloes and fringes (e.g. Figs 36, 37; PP2.2 is less problematic in this respect: Fig. 38). These artifacts can often be minimized through use of the ‘high pass’ filter in Photoshop, which, with suitable settings, can convert an image like the PP1 EDOF image of *Staurastrum* in Fig. 37 into one very similar to the PP2.2 image in Fig. 38. The illustrations of *Penium exiguum* West (Fig. 41) and *Tetmemorus* (Fig. 42) have both been improved by application of a high pass filter.

### Three-dimensional reconstruction

Figs 43 and 44 show two examples of Model 1 three-dimensional reconstruction, in which the original stack of  $x$ - $y$  slices along the  $z$  axis was rearranged into  $x$ - $z$  slices along the  $y$  axis and then run through the EDOF programs. The stacks used were those of the *Staurastrum* and *Penium* specimens shown in Figs 36 and 41. Because of diffraction, each small element of structure, such as the papillae of *S. cf. polymorphum*, appears not as a single dark or light spot but as a complex grey-scale pattern (cf. Figs 4, 5). Nevertheless, interpreted with reference to the EDOF image in the  $x$ - $y$  plane (Fig. 36), Fig. 43 can be seen to display the overall form of the *S. cf. polymorphum* cell, with four arms radiating from an ellipsoidal body. Likewise, Fig. 44 shows the circular section of *Penium exiguum*.

The 3-D shape of the *S. cf. polymorphum* cell is clearer in Figs 45 and 46, prepared using Model 2 methods from the same stack as Figs 25, 26. The in-focus pixels have been replotted as points in  $x$ - $y$  pixel  $\times$   $z$  slice space, with equal scaling in all dimensions, and the whole coordinate system rotated first in the  $x$ - $y$  plane (Fig. 45) and then orthogonally to show the shape of the cell in profile (Fig. 46). Using suitable graphics software, the semicell can be viewed from any angle.

With both Models, many parts of the cell wall are not represented in the re-orientations because they are gently curved and lay parallel to the plane of focus in the original image stack; being translucent, they therefore produced no detectable image. Hence, in Figs 43–46, the top and bottom faces of the *Staurastrum* and *Penium* semicells are represented only by local topographical features, such as granules and papillae.

### DISCUSSION

Published methods for preparing permanent mounts of desmids (e.g. Kopetzky-Rechtperg 1933; Alcorn 1935; Eckert 1949; van der Werff 1955; Brandham 1970) have not included a specific step for the removal of the cell contents, which is important for the visualization of taxonomic detail on the cell walls. The mountants used previously include euparal (Brandham 1970), pleurax (van der Werff 1955), caedax (Eckert 1949) or Canada balsam (Kopetzky-Rechtperg 1933; Alcorn 1935). The vast majority of desmid drawings, however, have been prepared from temporary mounts and either show the cells with their chloroplasts also present, or show the cell walls alone, with the cell contents omitted during drawing (e.g. Coesel 1982, 1983,

1985, 1991, 1994, 1997; Compère 2001; Croasdale & Flint 1986, 1988; Croasdale *et al.* 1983, 1994; Förster 1982; Lenzenweger 1996, 1997, 1999, 2003; Prescott *et al.* 1972, 1975, 1977, 1981, 1982; etc.). For photography of wall detail, however, removal of cell contents is desirable and our protocol does this effectively, producing clean desmid walls, which often separate into semicells. Occasional residual cell contents (e.g. Figs 29–32) probably cannot be avoided, because no preparation method is likely to be able to make a perfect separation between the cellulose wall and all other cell components.

Some collapse or distortion of walls was sometimes evident, but preservation was generally very good. No preparation method is likely to be equally suitable for all desmids and some modification may be necessary in particular cases. Diatoms and pollen grains provide useful parallels. Even well-tried methods for preparing diatom cell walls (e.g. Round *et al.* 1990) fail in some cases, destroying lightly silicified species (e.g. *Cylindrotheca*, some Cymatosiraceae) and causing fractures in a proportion of valves; indeed, in diatoms some degree of damage is often preferable, because it can separate the valves, which are used for identification, from the girdle bands, which generally are not. Preparation techniques for pollen grains (e.g. Moore & Webb 1978) also have differential effects and often lead to partial collapse or distortion of some grains.

Mountants such as euparal and Canada balsam (which is an alternative to euparal and could be used for desmids with only some slight modifications to the protocol, viz. elimination of residual water by transfer through absolute alcohol, alcohol–xylol, xylol, to Canada balsam) have proven longevity. Canada balsam slides of diatoms made by W. Smith or G. Walker-Arnott and held in the herbarium of the Royal Botanic Garden Edinburgh (E) are still essentially unchanged after 150 years. Hence, we are confident that our protocol will produce specimens of archival quality, suitable to act as types or authenticated material. Previously, if specimens were preserved at all, it was usually only as pickled or dried material (e.g. Brook 1959; Brook *et al.* 1993). Twenty years ago, Brook (1984) noted that the ‘iconotype has become accepted as the basis for the typification of taxa’ but that illustrations are ‘often poorly executed’. He suggested that this, together with a tendency to examine only a few specimens rather than well-sampled populations, was hindering the development of a satisfactory species-level taxonomy. A move to specimen-based typification would help to solve this problem. Even if authors prefer to continue to

typify desmids via drawings or other illustrations, rather than specimens, our protocol offers a new and better way to satisfy Recommendation 8A.1 of the International Code of Botanical Nomenclature (Greuter *et al.* 2000), that ‘when a holotype, a lectotype, or a neotype is an illustration, the specimen or specimens upon which that illustration is based should be used to help determine the application of the name’.

Illustrating types or other specimens in permanent preparations can of course be done by traditional means, viz. by drawing. However, although many desmidiologists are accomplished draughtsmen, our experience suggests that drawings by themselves are often not ideal for communication and identification. Fritsch (1953) said that the description and illustration of some desmids was ‘so inadequate that the forms in question are difficult or impossible to recognize’. Even where the standard of illustration is high, different authors have different drawing styles, as can be seen by comparing the detailed representations of *Staurastrum* species by Lenzenweger (1997), who shows the thickness of the cell wall as well as surface ornamentation, with the more simplified drawings of Lind & Brook (1980), Vyverman (1991), Croasdale *et al.* (1994, who often redrew the illustrations of other authors), Coesel (1997) or Ling & Tyler (2000). Furthermore, different amounts of detail are shown for what is said to be the same taxon. For example, in the monographs by West & West (1904–1923), very little information is given about the distribution of pores, whereas Williamson (e.g. 1996) records much more detail. Differences between the images of the same taxon are sometimes unavoidable because of changes in microscopy and increased knowledge (e.g. the better understanding of wall structure provided by scanning electron microscopy: Couté & Tell 1981), but they are also confusing, especially to the non-specialist, and they compromise consistent identification.

Replacing drawings with photographs has not previously been practical because of the depth-of-focus problem (e.g. see the very limited amount of information in each of Figs 1–3, 6, and the need for at least three images to create a barely adequate record of *Cosmarium margaritatum* in Figs 11–13). Few taxonomic accounts include significant photographic documentation, apart from Dürschmidt (1985). Three advances in information technology make photographic representation of desmids practical for taxonomic and other purposes. The first is digital imaging, which allows high quality images to be captured and processed quickly and easily

(although, without computer control of the focus control, building up image stacks is tedious) and reproduced accurately and infinitely. The second is electronic storage and dissemination via compact storage devices or the Internet, which together provide for low-cost archiving (relative to paper and film), as digitally-encoded information, and easy transmission of images over any distance. These two advances make it practical to distribute not only single images (which could already be done, through printed literature), but also stacks such as those used here (e.g. [http://rbg-web2.rbge.org.uk/DIADIST/focus/des\\_focus.htm](http://rbg-web2.rbge.org.uk/DIADIST/focus/des_focus.htm)) or those provided for diatom type specimens (of species of the diatoms *Diploneis* and *Sellaphora*, at <http://rbg-web2.rbge.org.uk/algae/research/types/types.htm>). Download times remain a constraint at present, but fast Internet connections are becoming more widely available. The third advance is the possibility we demonstrate here, to produce extended depth of focus images, from part or all of an image stack. This provides a summary image that can be used for initial comparisons, before the fine detail is examined via the stack.

The quality of our new EDOF images exceeds any we have seen for equivalent material and exceeds the results we have been able to achieve for our own image stacks using freeware or commercially available software. To reduce the graininess of our images it would be necessary to reduce the noise in the original images of the stacks, e.g. by increasing the exposure time or using greater bit-depth. We have provided several algorithms for construction of EDOF images, corresponding to PP1 and PP2.1–3, and the user must choose which performs best for particular purposes and material. Likewise, commercial software packages also often offer several algorithms, whose relative performance varies according to the kind of specimen being imaged.

A quite different method of producing EDOF images has been described that involves insertion of a special phase plate at the level of the condenser diaphragm (Dowski & Cathey 1995; Tucker *et al* 1999). This codes the wavefront in such a way that information from different planes within a specimen can afterwards be combined to produce an EDOF image by appropriate decoding of the digitally captured microscope image. However, although this approach may prove useful for microalgae, it is unclear that it is applicable to diffraction-limited microscopy of translucent material like desmid and diatom cell walls; nor does it yet provide the possibility of virtual reorientation that we demonstrate (Figs 43–46).

Our EDOF algorithms can identify the 3-D coordinates of wall structures, so that the specimen can subsequently be viewed along axes other than that originally selected. We readily acknowledge that the reorientations in Figs 43–46 are not ideal, but they are nevertheless informative (especially Fig. 46) and give an adequate impression of the profile of a semicell that has been photographed from a quite different angle. This is particularly important for highly three-dimensional taxa with radiating arms, such as many *Staurastrum* or *Stauroidesmus*. Virtual reorientation of EDOF images from conventional microscopy will never be wholly satisfactory until it is possible to remove diffraction artifacts, rather than partially circumvent them through pre-processing. Furthermore, producing a continuous contour for the reorientated cell wall, instead of an approximate profile created from the positions of spines and papillae, would require modelling, e.g. by introducing a requirement that all in-focus elements must be connected by a single, minimally curved basal surface). Nevertheless, most of the information needed to identify desmids to species or infraspecific level can be got from partial- or whole-stack EDOF images like those we present here, together with their admittedly imperfect virtual reorientations. Furthermore, if it were considered that EDOF images of a particular preserved type specimen were inadequate to represent all taxonomically relevant details, because the orientation of the specimen made it impossible to detect important features, it would always be possible to designate and illustrate epitypes to show these other aspects.

It has been suggested to us in review that laser scanning confocal microscopy of calcofluor-stained material (with addition of anti-fade compounds) might be a better alternative to our approach and it is true that virtual re-orientation of high resolution confocal images of fluorescent material (produced by staining or use of naturally fluorescence, e.g. of chloroplasts) is now routine. However, it is unlikely that such approaches can be applied to specimens mounted permanently in solid media and intended to serve as types for many decades. Fluorochromes generally have a short life, are bleached during observation, and could not be applied, or re-applied, to material that is already permanently mounted.

In future, EDOF images could be used for automated identification and this was the original motivation for our study. For diatoms, significant progress has recently been made towards automatic identification (Mann *et al.*, in press). The ADIAC project achieved ~ 96% success in trials, using single or paired images of diatoms (du Buf & Bayer 2002: pairs consist of an outline and a valve-face focus). In

the DIADIST project (<http://rbg-web2.rbge.org.uk/DIADIST/>), we have developed further algorithms that analyse shape and pattern for pennate diatoms (Hicks *et al.* 2004, 2006). We input grey-scale images of diatoms, perform Fourier analysis of the outline shape and internal pattern, and use the extracted data (~ 150 characters) to reconstruct the principal shape and pattern features in the form of a summary skeleton image (a ‘drawing’) of the outline and striae. Changes in shape, size and pattern during the life cycle and other phenotypic and genotypic variation within populations are modelled by using Principal Curves (Hastie & Stuetzel 1989) to characterize the main trends of variation (Hicks *et al.* 2004, 2006). The Principal Curve can then be used to produce drawings of ‘virtual’ specimens, which represent ‘typical’ members of the population, though none of the drawings will correspond exactly to any particular specimen. Desmids will require different shape and pattern descriptors, because most semicells are basically ellipsoids, rather than the relatively flat-topped box shapes of many diatoms. Furthermore, visual indexing will have to deal with the complication that the same taxon can vary from biradiate to multiradiate. On the other hand, desmids show less shape and size variation during the life cycle than diatoms. However, before visual indexing can be developed, it is essential to produce images that record and locate all relevant detail, despite the great depth of the cells relative to microscope depth of focus. The production of satisfactory EDOF images is thus an important first step towards visual indexing and unsupervised identification by computer.

#### **ACKNOWLEDGEMENTS**

This work was supported by BBSRC/EPSRC grant BIO14261. David Mann thanks the Royal Society for an equipment grant enabling purchase of a Reichert photomicroscope. We are grateful to Paul Hill, Nishan Canagarajah and Dave Bull from Bristol University for letting us use and modify their software to produce EDOF images in this article; and to Dr Ian Harding, Southampton Oceanography Centre, for very kindly running several image stacks through AutoMontage programs.

#### **REFERENCES**

ALCORN G.D. 1935. A new staining technique for desmids. *Stain Technology* 10: 107–108.

- BAYER M.M., DROOP S.J.M. & MANN D.G. 2001. Digital microscopy in phycological research, with special reference to microalgae. *Phycological Research* 49: 263–274.
- BICUDO C.E.M. & AZEVEDO M.T.P. 1977. Desmidióflora paulista I. Genero *Arthrodesmus* Ehr. ex Ralfs emend. *Arch. Bibliotheca Phycologica* 36: 1–105.
- BICUDO C.E.M. & DE CASTRO A.A.J. 1994. Desmidióflora paulista IV. Generos *Closterium*, *Spinoclosterium*. *Bibliotheca Phycologica* 95: 1–191.
- BICUDO C.E.M. & SAMANEZ Í.M. 1984. Desmidióflora paulista III. Generos *Bambusina*, *Desmidium*, *Groenbladia*, *Hyalotheca*, *Onychonema*, *Phymatodocis*, *Spondylosium*, *Teilingia*. *Bibliotheca Phycologica* 68: 1–139.
- BICUDO C.E.M. & SORMUS L. 1982. Desmidióflora paulista II. Genero *Micrasterias* C. Agardh ex Ralfs emend. *Arch. Bibliotheca Phycologica* 57: 1–230.
- BOURRELLY P. & COUTÉ A. 1991. Desmidiées de Madagascar (Chlorophyta, Zygomycetes). *Bibliotheca Phycologica* 86: 1–349.
- BRADBURY S. 1984. *An introduction to the optical microscope*. Oxford University Press, Oxford. 85 pp.
- BRANDHAM P.E. 1970. Techniques for the rapid preparation of permanent slides of microscopic algae. *British Phycological Journal* 5: 47–50.
- BROOK A.J. 1959. De Brébisson's determinations of *Staurastrum paradoxum* Meyen and *S. gracile* Ralfs. *Nova Hedwigia* 1: 163–166.
- BROOK A.J. 1981. *The biology of desmids*. Blackwell Scientific Publications, Oxford, UK. 276 pp.
- BROOK A.J. 1984. Comparative studies in a polyphyletic group, the Desmidiaceae – 30 years on. In: *Systematics of the green algae* (Ed. by D.E.G. Irvine & D.M. John), pp. 251–269. Academic Press, London.
- BROOK A.J., WILLIAMSON D.B. & SHOESMITH E. 1993. On the status of *Closterium abruptum* West and *Cl. nilssonii* Borge (Desmidiaceae: Zygomycetes). *Nova Hedwigia* 57: 255–268.
- BOURRELLY P. & COUTÉ A. 1991. Desmidiées de Madagascar (Chlorophyta, Zygomycetes). *Bibliotheca Phycologica* 86: 1–349.

- BUDAVARI S. (ed.) (1989). *The Merck Index*, ed. 11. Merck, Rahway, New Jersey.
- BURKE HUBBARD B. 1996. *The world according to wavelets: the story of a mathematical technique in the making*. A.K. Peters, Wellesley. 330 pp.
- BURT P.J. & KOLCZYNSKI R.J. 1993. Enhanced image capture through image fusion. *Proceedings of the 4<sup>th</sup> International Conference on Computer Vision (Berlin, Germany, May 11–14, 1993)*, pp. 173–182.
- COESEL P.F.M. 1982. *De Desmidiaceeën van Nederland – Sieralgen.*- Deel 1. *Fam. Mesotaeniaceae, Gonatozygaceae, Peniaceae*. Hoogwoud, The Netherlands. 32 pp.
- COESEL P.F.M. 1983. *De Desmidiaceeën van Nederland*. Deel 2. *Fam. Closteriaceae*. Hoogwoud, The Netherlands. 49 pp.
- COESEL P.F.M. 1985. *De Desmidiaceeën van Nederland*. Deel 3. *Fam. Desmidiaceae* (1). Koninklijke Nederlandse Natuurhistorische Vereniging, Utrecht, The Netherlands. 69 pp.
- COESEL P.F.M. 1991. *De Desmidiaceeën van Nederland*. Deel 4 *Fam. Desmidiaceae* (2). Koninklijke Nederlandse Natuurhistorische Vereniging, Utrecht, The Netherlands. 88 pp.
- COESEL P.F.M. 1994. *De Desmidiaceeën van Nederland*. Deel 5 *Fam. Desmidiaceae* (3). Koninklijke Nederlandse Natuurhistorische Vereniging, Utrecht, The Netherlands. 52 pp.
- COESEL P.F.M. 1996. Taxonomic notes on Dutch desmids III. *Cryptogamie, Algologie* 17: 19–34.
- COESEL P.F.M. 1997. *De Desmidiaceeën van Nederland*. Deel 6 *Fam. Desmidiaceae* (4). Koninklijke Nederlandse Natuurhistorische Vereniging, Utrecht, The Netherlands. 93 pp.
- COMPÈRE P. 2001. *Flore pratique des algues d'eau douce de Belgique: Desmidiées 1. Mesotaeniaceae, Gonatozygaceae, Peniaceae, Closteriaceae*. Jardin Botanique National de Belgique, Meise, Belgium. 69 pp.
- COUTÉ A. & DEHBI-ZEBBOUDJ A. 1988. *Cosmarium botrytis* (Menegh.) Ralfs var. *dayense* var. nov. (Chlorophyta, Zygothryxales, Desmidiaceae). *Cryptogamie, Algologie* 9: 149–155.

- COUTÉ A. & TELL G. 1981. Ultrastructure de la paroi cellulaire des Desmidiacées au microscope électronique à balayage. *Nova Hedwigia, Beiheft* 68: 1–228.
- CROASDALE H. & FLINT E.A. 1986. *Flora of New Zealand. Freshwater algae, Chlorophyta, desmids, with ecological comments on their habitats*, vol. 1. V.R. Ward, Wellington, New Zealand. 132 pp.
- CROASDALE H. & FLINT E.A. 1988. *Flora of New Zealand. Freshwater algae, Chlorophyta, desmids, with ecological comments on their habitats*, vol. 2. Actinotaenium, Cosmarium, Cosmocladium, Spinocosmarium, Xanthidium. Botany Division, D.S.I.R., Christchurch, New Zealand. 147 pp.
- CROASDALE H.T., BICUDO C.E.M. & PRESCOTT G.W. 1983. *A synopsis of the North American desmids. Part II. Desmidiaceae: Placodermae*, section 5. University of Nebraska Press, Lincoln, Nebraska, U.S.A.
- CROASDALE H., FLINT E.A. & RACINE M.M. 1994. *Flora of New Zealand. Freshwater algae, Chlorophyta, desmids, with ecological comments on their habitats*, vol. 3 Staurodesmus, Staurastrum and the filamentous desmids. Manaaki Whenua Press, Lincoln, Canterbury, New Zealand. 218 pp.
- DINGLEY M. 2003. William Joshua F.L.S., the unknown desmidiologist. *Biologia, Bratislava* 58: 723–727.
- DOWSKI E.R., JR. & CATHEY W.T. 1995. Extended depth of field through wave-front coding. *Applied Optics* 34: 1859–1866.
- DROOP S.J.M. 1996. The identity of *Diploneis splendida* (Bacillariophyta) and some related species. *Phycologia* 35: 404–420.
- DU BUF J.M.H. & BAYER M.M. (eds.) 2002. *Automatic Diatom Identification*. Series in Machine Perception and Artificial Intelligence, vol. 51. World Scientific Publishing, Singapore. 316 pp.
- DÜRRSCHMIDT M. 1985. Beitrag zur Kenntnis der Desmidiaceen des Bañado Cruces, Provinz Valdivia, Chile. *Bibliotheca Phycologica* 73: 1–138.
- ECKERT F. 1949. Desmidiaceen-Praeparation. *Mikrokosmos* 38: 89–92.
- FLEMING W.D. 1954. Naphrax: a synthetic mounting medium of high refractive index. New and improved methods of preparation. *Journal of the Royal Microscopical Society* 74: 42–44.

- FORSTER B., VAN DE VILLE D., BERENT J., SAGE D. & UNSER M. 2004. [Extended depth-of-focus for multi-channel microscopy images: a complex wavelet approach](#). In: *Proceedings of the Second IEEE International Symposium on Biomedical Imaging: Macro to Nano (ISBI 2004), 15-18 April 2004, Arlington, Virginia*, pp. 660-663. IEEE.
- FÖRSTER K. 1982. Conjugatophyceae: Zygnematales und Desmidiaceae (excl. Zygnemataceae). In: *Die Binnengewässer: Das Phytoplankton des Süßwassers. Systematik und Biologie*, vol. 8, part 1 (Ed. by G. Huber-Pestalozzi), pp. 1–543. E. Schweizerbart'sche Verlagsbuchhandlung, Stuttgart.
- FREY-WYSSLING A. 1976. *The plant cell wall*. Gebrüder Borntraeger, Berlin and Stuttgart. 294 pp.
- FRITSCH F.E. 1953. Comparative studies in a polyphyletic group, the Desmidiaceae. *Proceedings of the Linnean Society of London* 164: 258–280.
- GERRATH J.F. 1993. The biology of desmids: a decade of progress. *Progress in Phycological Research* 9: 79–192.
- GERRATH J.F. & JOHN D.M. 1991. Desmids of Ghana, West Africa II. *Cosmarium*, *Staurastrum* and other genera. *Nova Hedwigia* 52: 375–410.
- GONTCHAROV A.A. & MELKONIAN M. 2005. Molecular phylogeny of *Staurastrum* Meyen ex Ralfs and related genera (Zygnematophyceae, Streptophyta) based on coding and noncoding rDNAa sequence comparisons. *Journal of Phycology* 41: 887–899.
- GONTCHAROV A.A., MARIN B. & MELKONIAN M. 2002. Molecular phylogeny of conjugating green algae (Zygnemophyceae, Streptophyta) inferred from SSU rDNA sequence comparisons. *Journal of Molecular Evolution* 56: 89–104.
- GONZALEZ R.C. & WINTZ P. 1987. *Digital image processing*, ed 2. Addison–Wesley, Reading, Massachusetts, U.S.A.
- GRAHAM L.E. & WILCOX L.W. 2000. *Algae*. Prentice–Hall, Upper Saddle River, New Jersey. 640 pp.
- GREUTER W., BARRIE F.R., BURDET H.-M., DEMOULIN V., FILGUEIRAS S., NICOLSON D.H., SILVA P.C., SKOG J.E., TREHANE P., TURLAND N.J. & HAWKSWORTH D.L. 2000. [International Code of Botanical Nomenclature \(St. Louis Code\)](#). Koeltz Scientific Books, Königstein. 474 pp.

- HASTIE T. & STUETZEL W. 1989. Principal Curves. *Journal of the American Statistical Association* 84: 502–516.
- HEGEWALD E. & FEHER G. 2003. Studies on bi- and triradiate isolates of the *Staurastrum teliferum–gladiosum* complex and their phylogenetic position. *Biologia*, Bratislava 58: 665–670.
- HICKS Y., MARSHALL D., MARTIN R.R., ROSIN P.L., DROOP S. & MANN D.G. 2004. Building shape and texture models of diatoms for analysis and synthesis of drawings and identification. In: *Proceedings of the Irish Machine Vision and Image Processing Conference (IMVIP 2004)* (Ed. by K.Dawson-Howe, A.C. Kokaram & F.Shevlin), pp. 26–33. Trinity College Dublin, Ireland.
- HICKS Y.A., MARSHALL D., ROSIN P.L., MARTIN R.R., MANN D.G. & DROOP S.J.M., 2006, in press. A model of diatom shape and texture for analysis, synthesis and identification. *Machine Vision and Applications Journal*
- HILL P., CANAGARAJAH N. & BULL D. 2002. Image fusion using complex wavelets. In: *Proceedings of the British Machine Vision Conference (BMVC 2002)*, 2-5 September, 2002, Cardiff, UK (Ed. by D. Marshall & P.L. Rosin), pp. 487–496. British Machine Vision Association.
- JOHN D.M., WHITTON B.A. & BROOK A.J. 2002. *The freshwater algal flora of the British Isles. An identification guide to freshwater and terrestrial algae.* Cambridge University Press, Cambridge. 702 pp and CD-ROM.
- KIM H.S. 1996. Desmids (*Staurastrum* and *Stauroidesmus*) from Kyongsangnam-Do, Korea. *Nova Hedwigia* 62: 521–541.
- KOPETZKY-RECHTER O. 1933. Erfahrungen bei der Herstellung von Desmidiaceen-Dauerpräparaten. *Mikrokosmos* 26: 141-144.
- KOUWETS F.A.C. 1991. Notes on the morphology and taxonomy of some rare or remarkable desmids (Chlorophyta, Zygnemaphyceae) from south-west France. *Nova Hedwigia* 53: 383–408.
- KOUWETS F.A.C. & COESEL P.F.M. 1984. Taxonomic revision of the Conjugatophycean family Peniaceae on the basis of cell wall ultrastructure. *Journal of Phycology* 20: 555–562.
- LENZENWEGER R. 1996.. Desmidiaceenflora von Österreich. Teil 1. *Bibliotheca Phycologica* 101: 1–162.

- LENZENWEGER R. 1997. Desmidiaceenflora von Österreich. Teil 2. *Bibliotheca Phycologica* 102: 1–216.
- LENZENWEGER R. 1999. Desmidiaceenflora von Österreich. Teil 3. *Bibliotheca Phycologica* 104: 1–218.
- LENZENWEGER R. 2003. Desmidiaceenflora von Österreich. Teil 4. *Bibliotheca Phycologica* 111: 1–87.
- LEWIN J.C. 1962. Silicification. In: *Physiology and biochemistry of algae* (Ed. by R.A. Lewin), pp. 445–453. Academic Press, New York and London.
- LI H., MANJUNATH B.S. & MITRA S.K. 1995. Multisensor image fusion using the wavelet transform. *Graphical Models and Image Processing* 57: 233–245.
- LIND E.M. & BROOK A.J. 1980. *Desmids of the English Lake District*. Scientific Publication no. 42, Freshwater Biological Association, Ambleside, UK. 123 pp.
- LING H.U. & TYLER P.A. 2000. Australian freshwater algae (exclusive of diatoms). *Bibliotheca Phycologica* 105: 1–643.
- MANN D.G. 1998. Ehrenbergiana: problems of elusive types and old collections, with special reference to diatoms. *Linnean, Special Issue* 1: 63–88
- MANN D.G. 2002. The systematics of the *Sellaphora pupula* complex: typification of *S. pupula*. In: *Lange-Bertalot Festschrift* (Ed. by R. Jahn, J.P. Kociolek, A. Witkowski & P. Compère), pp. 225–242. A.R.G. Gantner Verlag, Liechtenstein.
- MANN, D.G., DROOP, S.J.M., HICKS, Y.A., MARSHALL, A.D., MARTIN, R.R. & ROSIN, P.L. (in press). Alleviating the taxonomic impediment in diatoms: prospects for automatic and web- based identification systems. In: *Proceedings of the 18th International Diatom Symposium* (Ed. by A. Witkowski). Biopress, Bristol.
- MCCOURT R.M., KAROL K.G., BELL J., HELM-BYCHOWSKI K.M., GRAJEWSKA K., WOJCIECHOWSKI K.F. & HOSHAW R.W. 2000. Phylogeny of the conjugating green algae (Zygnemophyceae) based on rbcL sequences. *Journal of Phycology* 36: 747–758.
- MOORE P.D. & WEBB J.A. 1978. *Illustrated guide to pollen analysis*. Hodder & Stoughton, London. 192 pp.

- PLUTA M. 1993. *Advanced light microscopy*, vol. 3. *Measuring techniques*. Elsevier, Amsterdam. 702 pp.
- PRESCOTT G.W., CROASDALE H.T. & VINYARD W.C. 1972. *A synopsis of North American desmids*. Part 1. *Saccodermæ*. New York Botanical Garden, New York.
- PRESCOTT G.W., CROASDALE H.T. & VINYARD W.C. 1975. *A synopsis of the North American desmids*. Part II. *Desmidiaceae: Placodermæ*, section 1. University of Nebraska Press, Lincoln, Nebraska, U.S.A.
- PRESCOTT G.W., CROASDALE H.T. & VINYARD W.C. 1977. *A synopsis of the North American desmids*. Part II. *Desmidiaceae: Placodermæ*, section 2. University of Nebraska Press, Lincoln, Nebraska, U.S.A.
- PRESCOTT G.W., CROASDALE H.T., VINYARD W.C. & BICUDO C.E.M. 1981. *A synopsis of the North American desmids*. Part II. *Desmidiaceae: Placodermæ*, section 3. University of Nebraska Press, Lincoln, Nebraska, U.S.A.
- PRESCOTT G.W., BICUDO C.E.M. & VINYARD W.C. 1982. *A synopsis of the North American desmids*. Part II. *Desmidiaceae: Placodermæ*, section 4. University of Nebraska Press, Lincoln, Nebraska, U.S.A.
- RALFS J. 1848. *The British Desmidiæeae*. Reeve, Benham & Reeve, London. 226 pp.
- ROUND F.E. 1953. An investigation of two benthic algal communities in Malham Tarn, Yorkshire. *Journal of Ecology* 41: 174–197.
- ROUND F.E., CRAWFORD R.M. & MANN D.G. 1990. *The diatoms. Biology & morphology of the genera*. Cambridge University Press, Cambridge. 747 pp.
- RŮŽIČKA J. 1977. *Die Desmidiaceen Mitteleuropas*. Band 1, 1. Lieferung. E. Schweizerbart'sche Verlagsbuchhandlung, Stuttgart, Germany. 292 pp.
- RŮŽIČKA J. 1981. *Die Desmidiaceen Mitteleuropas*. Band 1, 2. Lieferung. E. Schweizerbart'sche Verlagsbuchhandlung, Stuttgart, Germany. 736 pp.
- TUCKER S.C., CATHEY W.T. & DOWSKI E.R., JR. 1999. Extended depth of field and aberration control for inexpensive digital microscope systems. *Optics Express* 4: 467–474.

- VALDESCAS A.G., MARSHALL D., BECERRA J.M. & TERRERO J.J. 2001. On the extended depth of focus algorithms for brightfield microscopy. *Micron* 32: 559–569.
- VAN DEN HOEK C., MANN D.G. & JAHNS H.M. 1995. *Algae. An introduction to phycology*. Cambridge University Press, Cambridge. 623 pp.
- VAN DER WERFF A. 1955. A new method of concentrating and cleaning diatoms and other organisms. *Verhandlungen der Internationalen Vereinigung für theoretische und angewandte Limnologie* 12: 276–277.
- VYVERMAN W. 1991. Desmids from Papua New Guinea. *Bibliotheca Phycologica* 87: 1–201.
- WEST W. & WEST G.S. 1904–1923. *A monograph of the British Desmidiaceae*, vols 1–5. The Ray Society, London.
- WILLIAMSON D.B. 1996. A survey of the desmid flora of Assynt, West Sutherland. *Botanical Journal of Scotland* 48: 235–279.
- WILLIAMSON D.B. 1997. Rare desmids from Scotland. *Archiv für Hydrobiologie* 118 (*Algological Studies* 84): 53–81.
- YOUNG I.T., ZAGERS R., VAN VLIET L.J., MULLIKIN J., BODDEKE F.R. & NETTEN H. 1993. [Depth-of-focus in microscopy](#). In: *Proceedings of the 8th Scandinavian Conference on Image Analysis* (Tromsø, Norway, May 25-28, 1993), pp. 493–498. Norwegian Society for Image Processing and Pattern Recognition, Tromsø, Norway.

## FIGURE LEGENDS

**Fig. 1.** *Staurastrum cf. teliferum*, differential interference contrast optics: apex of semi cell, showing fine pores at the semicell apex, arranged in two concentric rings (the outer one rather more irregular) around a single central pore. Scale bar = 10  $\mu\text{m}$

**Fig. 2.** *Staurastrum cf. polymorphum*, bright field optics. Note that the left two arms are in black focus, whereas the right two arms are just beyond their white focus. Scale bar = 10  $\mu\text{m}$ .

**Fig. 3.** *Staurastrum cf. polymorphum*, phase contrast optics. The left arms are in black focus and the right hand arms are almost in white focus below the focal plane; the isthmus and surrounding papillae are also in white focus, but lie above the focal plane. Scale bar = 10  $\mu\text{m}$ .

**Figs 4, 5.** Imaging of small objects (embedded in a medium of lower refractive index), showing the effects of diffraction. The images are vertical ‘sections’ through stacks of  $x$ - $y$  optical sections (see text). Scale bar = 10  $\mu\text{m}$

**Fig. 4.** Bright field optics, showing the formation of two in-focus images, one white, one black (arrows), separated by a shallow zone of uncertainty. As the microscope is focused down onto an object (vertically downwards in Fig. 4), the object first appears white, becoming sharper as the focal plane of the objective gets closer to the object plane. It then disappears briefly, before reappearing in sharp black focus. Note that the principal foci (white or black) are surrounded by narrow cones of opposite phase.

**Fig. 5.** Phase contrast optics. The object is black and in focus at the focal plane (middle arrow); some vertical distance away from the focal plane in either direction, the object disappears, then reappears in white focus (upper and lower arrows), then becomes progressively out of focus with increasing distance from the focal plane.

**Figs 6–8.** *Staurastrum cf. polymorphum*. A single optical section (bright-field optics), focused on a ring of papillae near the isthmus, showing the effects of image pre-processing. All three images have been given exactly the same contrast and brightness enhancement. Scale bar = 10  $\mu\text{m}$ .

**Fig. 6.** Original image. Because the semicell was lying slightly oblique to the image plane, some papillae are in white focus (e.g. arrows), whereas others are in black focus (e.g. arrowhead).

**Fig. 7.** Image after pre-processing by method PP1. Papillae originally in white focus now appear black (arrows); papillae that were originally black remain black but gain a dark halo (arrowhead).

**Fig. 8.** Image after pre-processing by method PP.1. The white-focus elements have been virtually eliminated (e.g. arrows); papillae in black focus remain almost unaltered in appearance (arrowhead).

**Figs 9–23.** Cell walls of placoderm desmids prepared using the new protocol, differential interference contrast optics. Scale bars = 20  $\mu\text{m}$ .

**Figs 9, 10.** *Micrasterias thomasi* Archer semicell.

**Figs 11–13.** *Cosmarium margaritatum* Lundell f. *subrotundatum* Roy & Bissett, whole cell.

**Figs 14, 15.** *Euastrum* cf. *obesum* Joshua, whole cell.

**Figs 16, 17.** *Euastrum* cf. *bidentatum* Nägeli, whole cell.

**Figs 18, 19.** *Cosmarium furcatospermum* West & G.S. West, whole cell.

**Figs 20, 21.** *Cosmarium ornatum* Ralfs, semicell.

**Figs 22, 23.** *Pleurotaenium ehrenbergii* (Brébisson) De Bary, semicell.

**Fig. 24.** *Staurastrum* cf. *polymorphum*. Bright-field EDOF image prepared without pre-processing. Comparison with Figs 25–28, 34 and 35 shows that many papillae are either poorly imaged or lost altogether. Scale bar = 10  $\mu\text{m}$

**Figs 25–28.** *Staurastrum* cf. *polymorphum*. EDOF images of a semicell in apical view. Scale bar = 10  $\mu\text{m}$ .

**Fig. 25.** Bright field optics, stack pre-processed according to PP1.

**Fig. 26.** Bright field optics, stack pre-processed according to PP2.1.

**Fig. 27.** Phase contrast optics, stack pre-processed according to PP1.

**Fig. 28.** Phase contrast optics, stack pre-processed according to PP2.1.

**Figs 29–32.** *Staurastrum cf. teliferum*. EDOF images of a semicell in apical view. Scale bar = 10  $\mu\text{m}$ .

**Fig. 29.** Bright field optics, stack pre-processed according to PP1.

**Fig. 30.** Bright field optics, stack pre-processed according to PP2.1.

**Fig. 31.** Phase contrast optics, stack pre-processed according to PP1.

**Fig. 32.** Phase contrast optics, stack pre-processed according to PP2.1.

**Figs 33–35.** *Staurastrum cf. polymorphum*, semicell in apical view, EDOF images. Scale bar = 10  $\mu\text{m}$ .

**Fig. 33.** Image produced from the same bright-field image stack as Figs 25–28, but using Auto-Montage software. Note the mosaic of incompletely fused image segments around the margin and the inconsistent rendering of papillae.

**Fig. 34.** Isthmus face of semicell, phase contrast optics, from a subset of the stack used for Figs 27, 28. Note the clear visualization of the ring of papillae around the isthmus.

**Fig. 35.** As Fig. 34, but derived from a different subset of optical sections and showing the apical face of semicell.

**Figs 36–42.** Examples of EDOF images derived from partial or whole stacks. Scale bar = 10  $\mu\text{m}$ .

**Fig. 36.** *Staurastrum cf. polymorphum*. Semicell lying obliquely, phase contrast optics, whole stack pre-processed by PP1. The isthmus aperture is not fully defined.

**Fig. 37.** *Staurastrum cf. polymorphum*. Cell in side view, phase contrast optics, whole stack, pre-processed by PP1. Further post-processing,

e.g. by high pass filter, can remove the prominent fringes present around the cell and the darker areas within each semicell.

**Fig. 38.** As Fig. 37, but with PP2.2 pre-processing, producing an image that resembles a line drawing and contains much the same information.

**Fig. 39.** *Euastrum bidentatum*. Partial stack showing one side of a whole cell in face view; phase contrast optics, PP2.1 pre-processing. Note the central ring of granules and other isolated granules lying near each lobe.

**Fig. 40.** *Cosmarium sexnotatum* Gutwinski. Whole cell in side view, phase contrast optics, PP1 pre-processing: partial stack, showing only one side of the cell. The three or four longitudinal ridges at the centre of each semicell are just visible, together with lines of two or three pores between them .

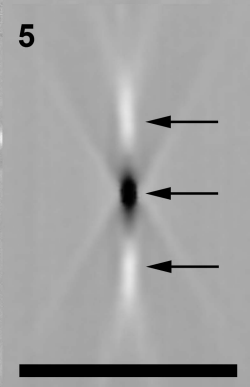
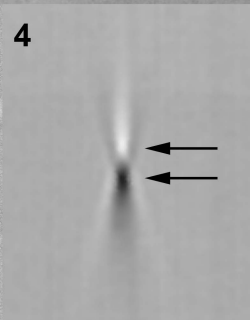
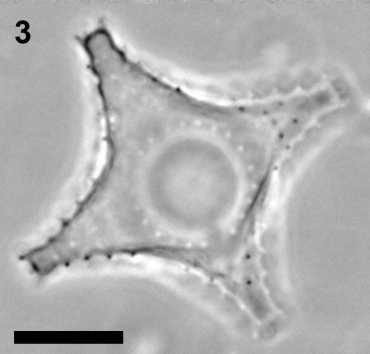
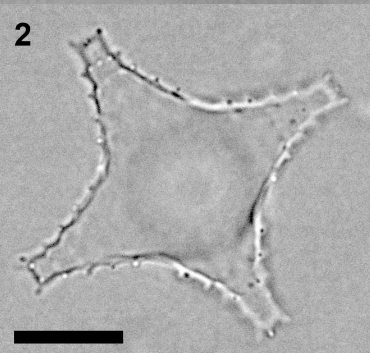
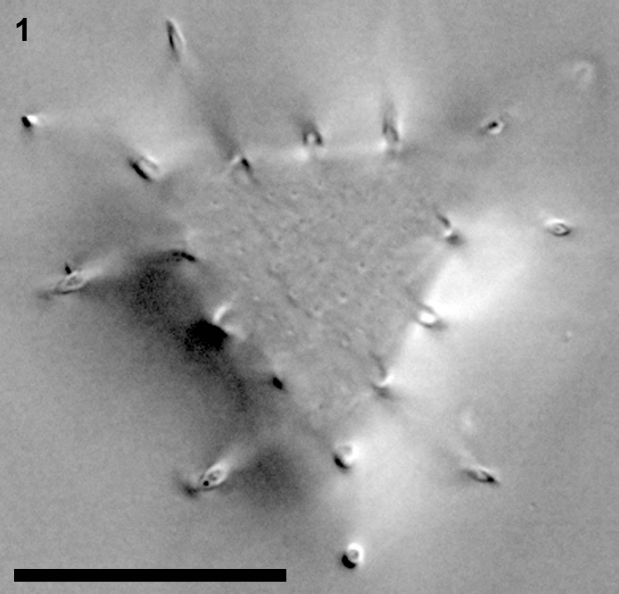
**Fig. 41.** *Penium exiguum*. Whole cell in side view, phase contrast optics, PP2.3 processing: partial stack, showing only one side of the cell, which is covered with short blunt spines.

**Fig. 42.** *Tetmemorus brebissonii* (Meneghini) Ralfs. Semicell in side view, phase contrast optics, PP1 pre-processing: the whole stack was used, representing both sides of the semicell.

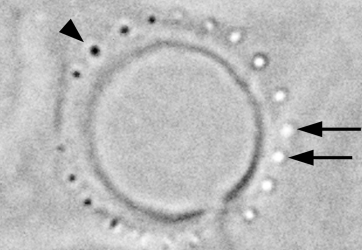
**Fig. 43.** EDOF image derived from the *Staurastrum cf. polymorphum* stack used to produce Fig. 36, after orthogonal transformation to produce a new stack of  $x-z$  images along the  $y$  axis. The image has been re-scaled to correct for the different (lower) spacing along the  $z$  axis, in effect producing cubic voxels. The ends of the four arms of the semicell are visible (arrows). Scale bar = 10  $\mu\text{m}$ .

**Fig. 44.** EDOF image derived from the *Penium* used to produce Fig. 41 (except that the whole stack was analysed, not simply the top half), after orthogonal transformation to produce a new stack of  $x-z$  images along the  $y$  axis. The image has been re-scaled as in Fig. 39 and shows the circular cross section of *Penium*. Scale bar = 10  $\mu\text{m}$ .

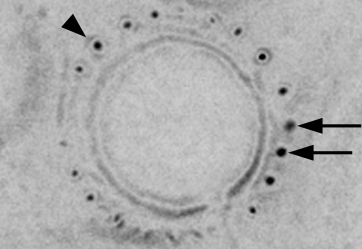
**Figs 45, 46.** *Staurastrum cf. polymorphum*: in-focus pixels from the Fig. 25–28 stack plotted in the  $x$ - $y$  plane with rotation to form a new  $x'$ - $y'$  coordinate system (Fig. 45), and then rotation around the  $x'$  axis to give a projection of the desmid in the  $y'$ - $z$  plane (Fig. 46) The axes are scaled equally;  $x$  and  $y$  are calibrated in pixels of the original image.



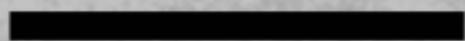
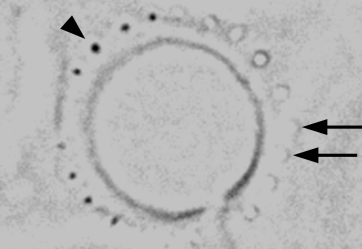
6

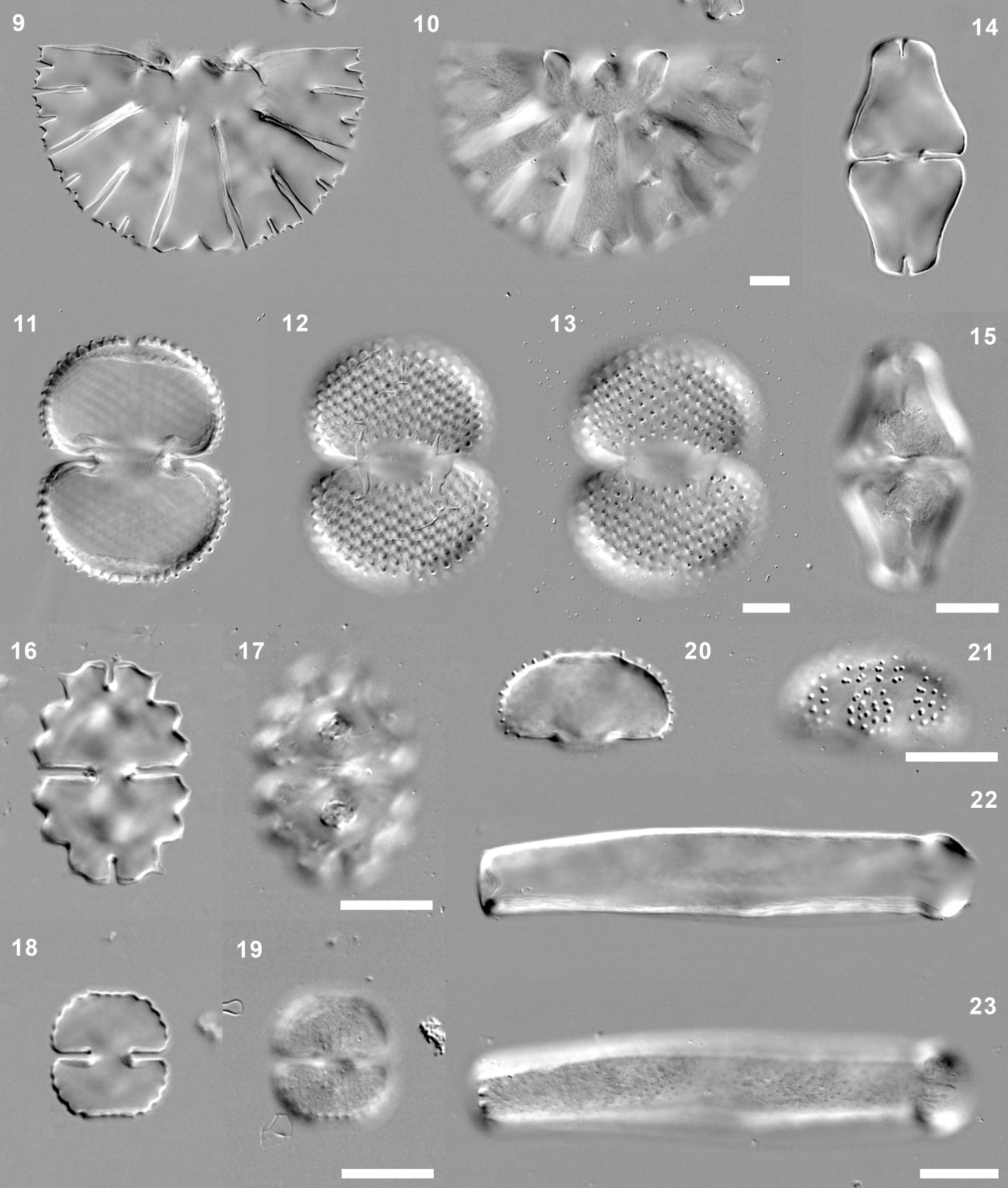


7

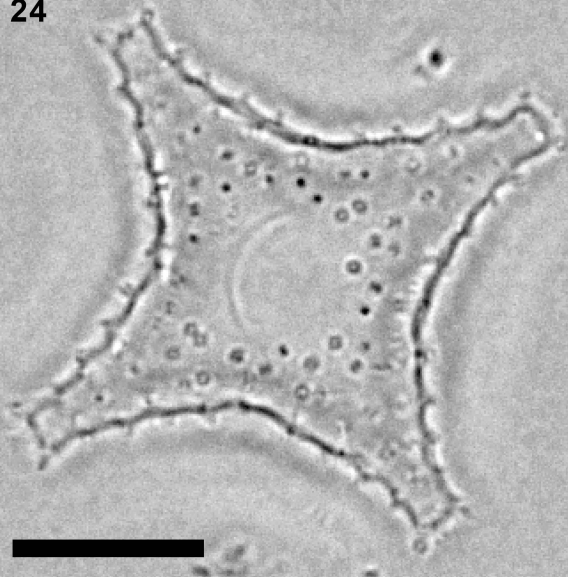


8

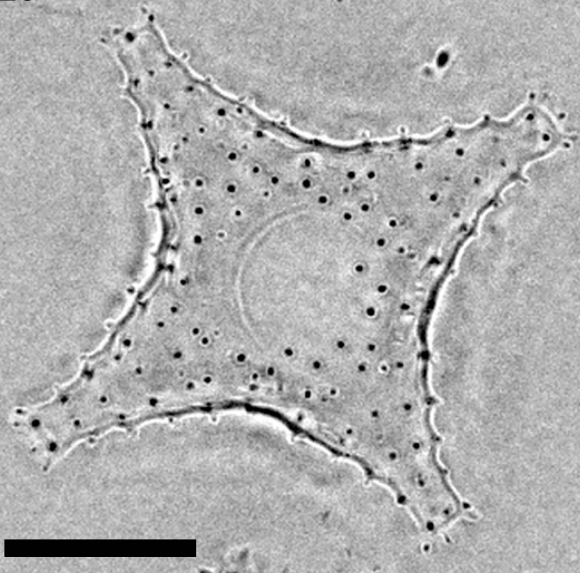




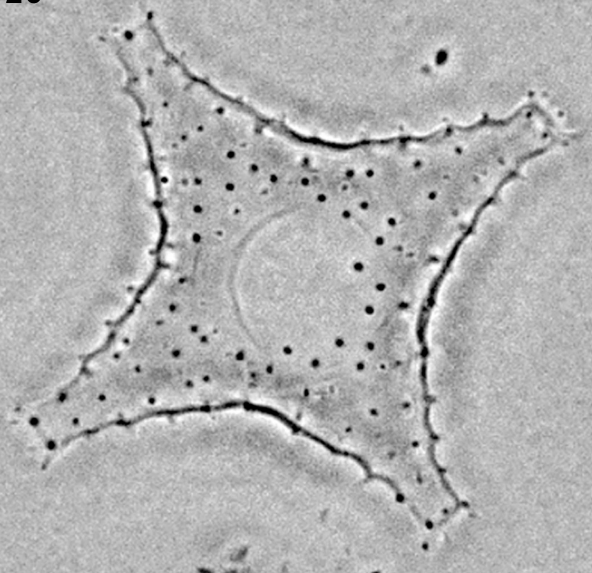
24



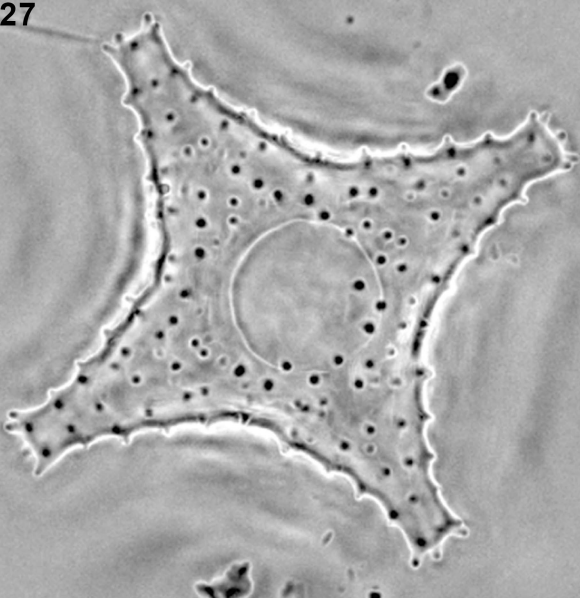
25



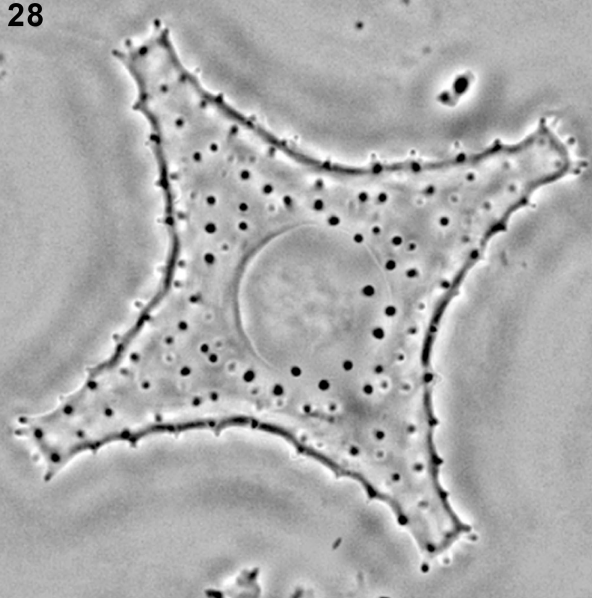
26



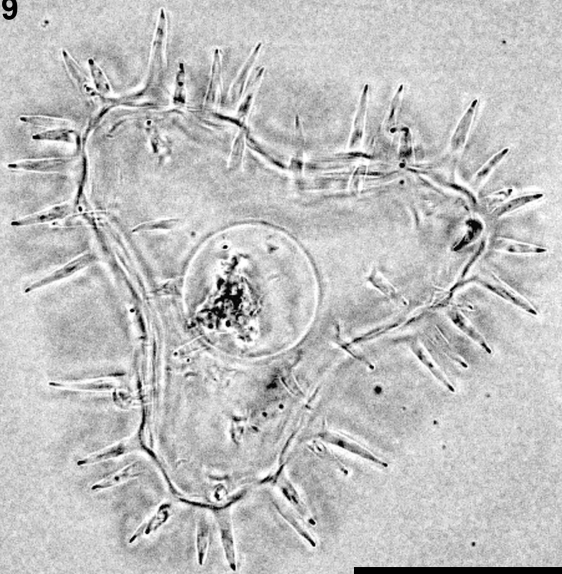
27



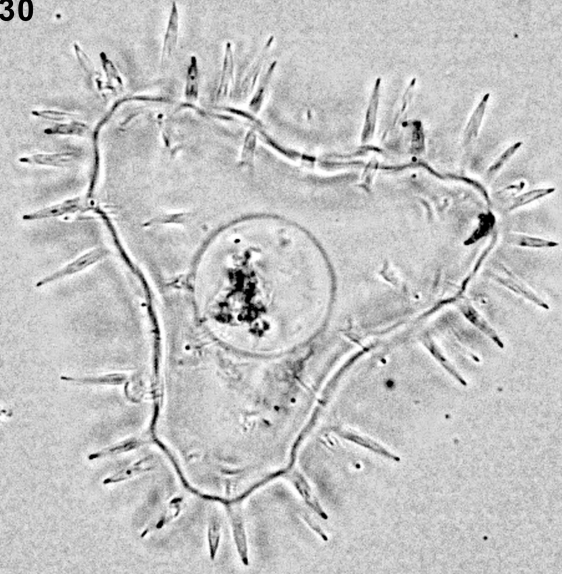
28



29



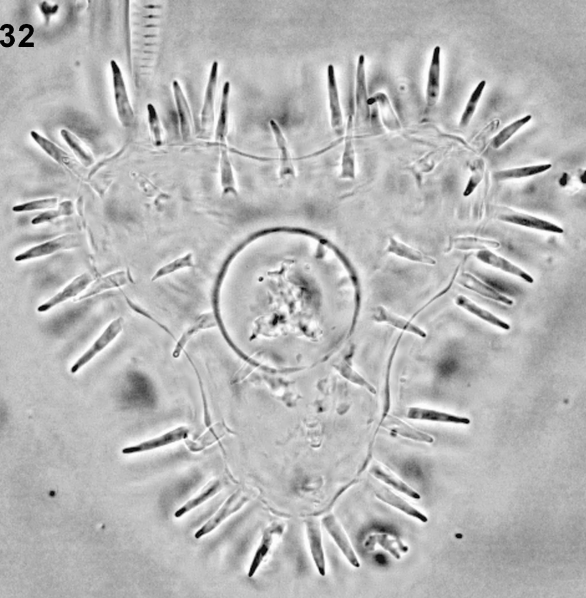
30



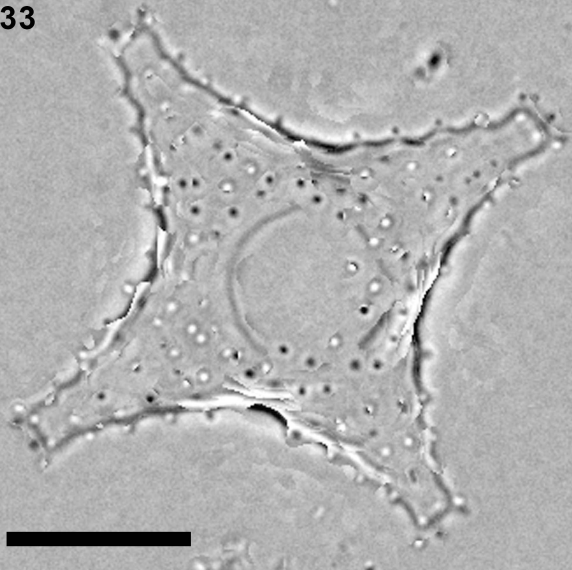
31



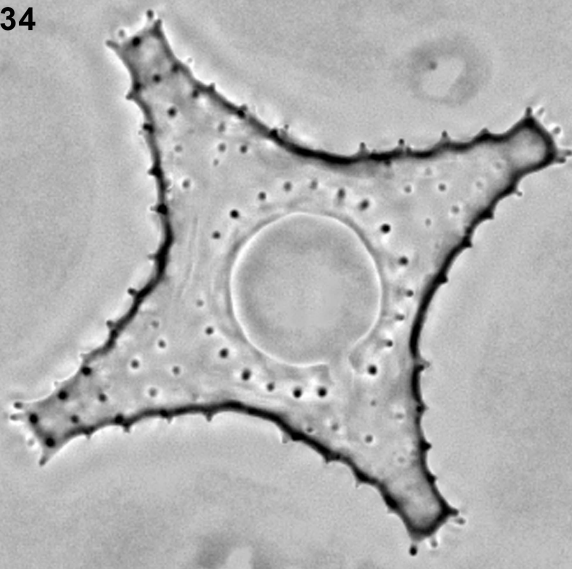
32



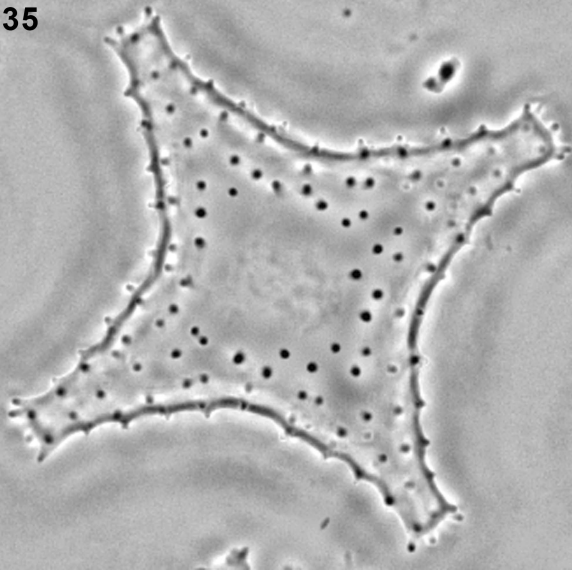
33

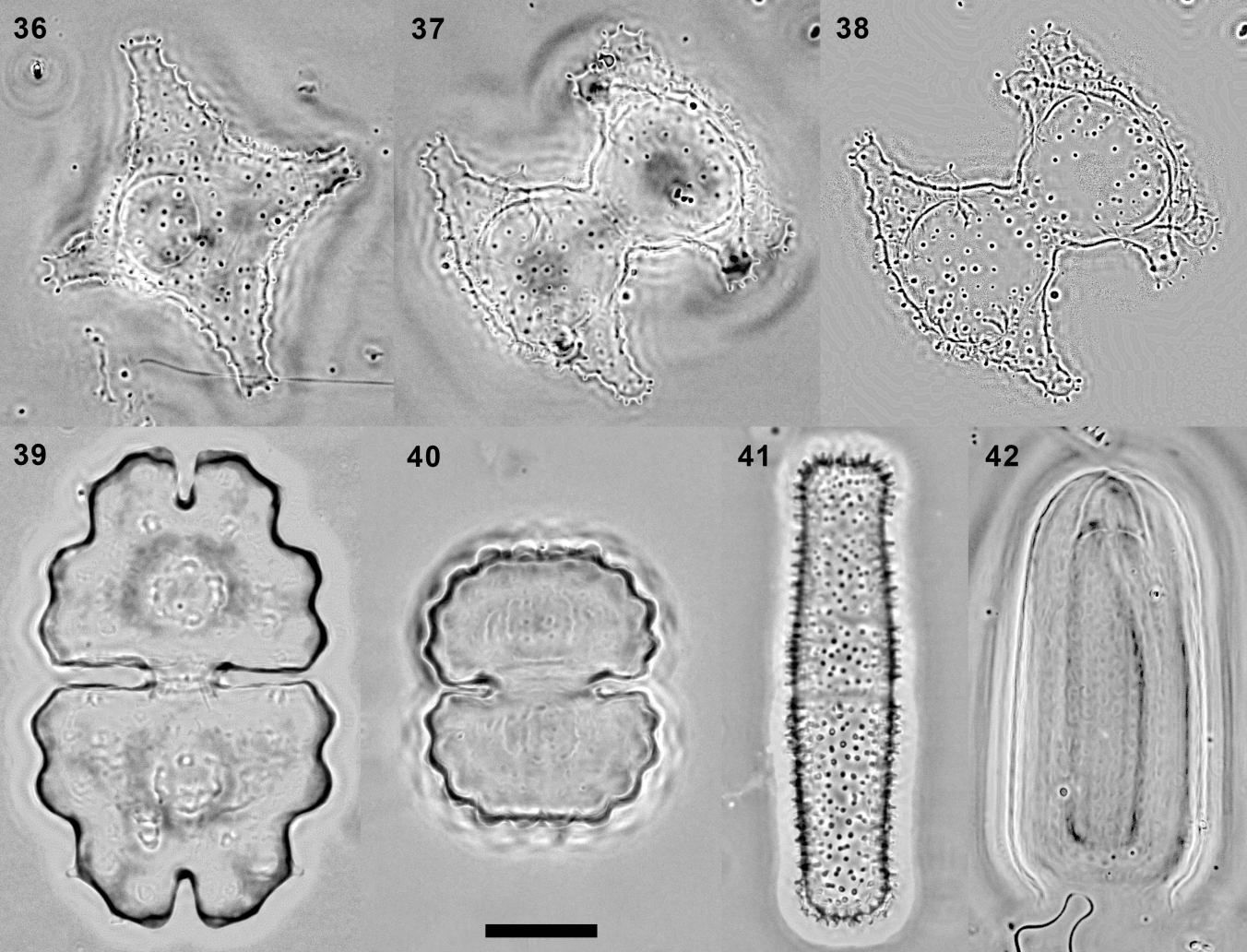


34

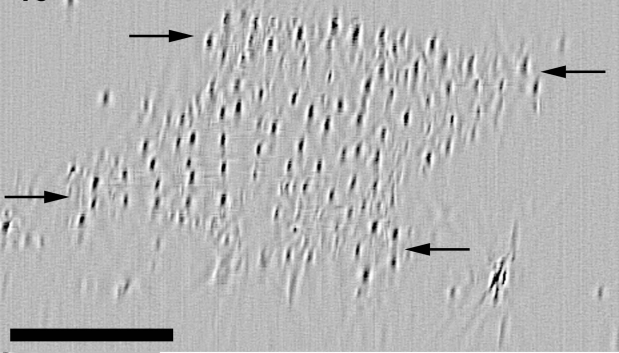


35

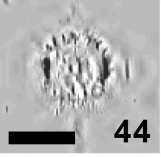




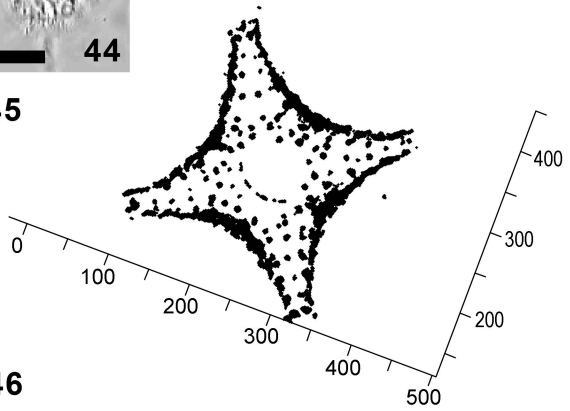
43



44



45



46

